Chem

CellPress

Article

# Geminal Dimethyl Substitution Enables Controlled Polymerization of Penicillamine-Derived β-Thiolactones and Reversed Depolymerization

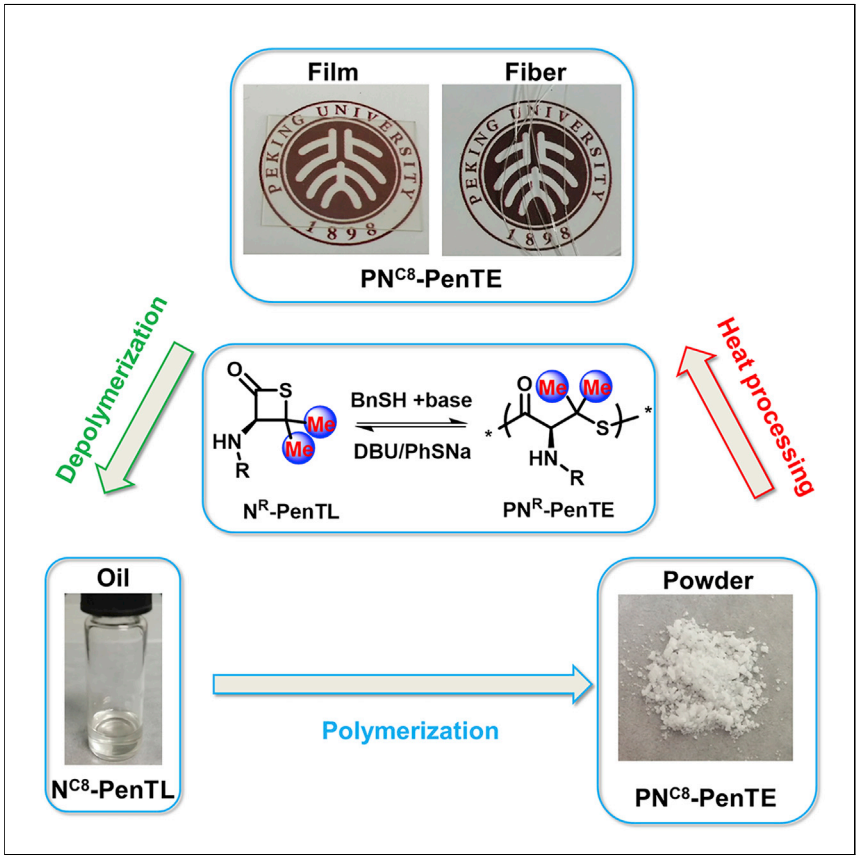


Polythioesters are promising candidates as sustainable polymers, but their controlled and selective (de)polymerization remains a significant challenge. In the current study, we addressed this problem by designing a thermodynamically neutral and kinetically trapped system based on penecillamine-derived β-thiolactones, opening the possibility of establishing a circular economy for plastic materials.

Wei Xiong, Wenying Chang, Dong Shi, ..., Xuhao Zhou, Er-Qiang Chen, Hua Lu

eqchen@pku.edu.cn (E.-Q.C.)
chemhualu@pku.edu.cn (H.L.)

## HIGHLIGHTS

Highly controlled polymerization using *gem*-dimethyl substituted β-thiolactones

Efficient depolymerization due to a conformationally constrained terminal thiol

Semicrystalline polythioesters with high molar mass and tunable mechanical properties

Thorpe-Ingold effect for tuning the reversibility of ring-opening polymerization

Xiong et al., Chem *6*, 1831–1843
July 9, 2020 
https://doi.org/10.1016/j.chempr.2020.06.003

Chem

CellPress

Article

# Geminal Dimethyl Substitution Enables Controlled Polymerization of Penicillamine-Derived β-Thiolactones and Reversed Depolymerization

Wei Xiong,[1] Wenying Chang,[1] Dong Shi,[1] Lijiang Yang,[2] Ziyou Tian,[1] Hao Wang,[1] Zhengchu Zhang,[1] Xuhao Zhou,[1] Er-Qiang Chen,[1,*] and Hua Lu[1,3,*]

## SUMMARY

**To access infinitely recyclable plastics, one appealing approach is to design thermodynamically neutral systems based on dynamic covalent bond, the (de)polymerization of which can be easily manipulated with low energy cost. Here, we demonstrate the feasibility of this concept via the efficient synthesis of polythioesters $PN^R$-PenTE from penicillamine-derived β-thiolactones and their convenient depolymerization under mild conditions. The *gem*-dimethyl group adjusts the thermodynamics of (de)polymerization to near equilibrium, confers better (de)polymerization control by reducing the activity and conformational possibilities of the chain-end thiolate groups, and stabilizes the thioester linkages in the polymer backbone. $PN^R$-PenTE with tailored properties is conveniently accessible by altering the side chains. $PN^R$-PenTE can be recycled to pristine enantiopure β-thiolactones at >95% conversion from minutes to a few hours at room temperature. This work highlights the power of judicious molecular design and could greatly facilitate the development of a wide range of recyclable polymers with immense application potentials.**

## INTRODUCTION

The annual global production of plastics has increased more than 20-fold since 1964, reaching 348 million metric tons in 2017.[1] The rapid accumulation of petroleum-based plastic wastes has created one of the greatest environmental crises in the world.[2] Single-use plastics have been banned in Europe, while other countries (e.g., China) are expected to enact similar regulations in the near future. In conjunction to developing methodologies for the degradation of existing plastics,[3–5] the need for infinitely recyclable new plastics from renewable feedstock has received vast global attention.[6–12] As previously suggested by Endo, Albertsson, and others, one of the many appealing strategies is to design thermodynamically near-equilibrium systems for easy manipulation of the polymerization and reverse depolymerization.[13–17] Along this direction, many biomass and $CO_2$ derived synthetic polymers, mainly polyesters and polycarbonates, have shown their capability of establishing a circular economy of monomer-polymer-monomer.[18–34] Despite the advancement, the development of recyclable polymers under mild condition and at low energy cost have been limited. Some of the thermodynamically neutral systems may suffer from low selectivity in monomer recovery as a result of the generation of oligomeric mixtures, thus necessitating extra work to push the equilibrium towards monomer formation. Kinetically trapped polymers such as poly(γ-butyrolactone) can be completely recycled, elegantly demonstrated by Chen et al., but the polymerization

### The Bigger Picture

Chemically recyclable polymers from renewable feedstock hold great promise for solving the imminent global plastic-waste crisis. Despite recent advances, challenges including high energy consumption, the limited choices of sustainable polymers, and side reactions that could hamper complete monomer recovery are still yet to be addressed. By introducing a *gem*-dimethyl substitution, we succeeded in regulating both the forward polymerization of β-thiolactones and the backward depolymerization of polythioesters in a highly controlled fashion and with low energy input. Moreover, our strategy allows facile access to semicrystalline plastics with tailorable mechanical and thermal properties from biorenewable penicillamine feedstock. We envision that our design principle can facilitate the development of a new generation of chemically recyclable polythioester-based polymers, providing a sustainable solution to the ongoing environmental and economic challenge caused by nondegradable plastics.

of the non-strained γ-butyrolactone requires very low temperatures (−30°C to −60°C) because of unfavorable thermodynamics ($\Delta G_P^\circ$ = + 6.4 kJ/mol). Moreover, both the polymerization and depolymerization need strong catalysts and demanding conditions because of the relatively high energy barrier for ester activation.[19,31] Thus, introducing more dynamic bonds to thermodynamically near-equilibrium system could be a viable but underdeveloped approach to design sustainable polymers.

Polythioesters (PTE) are one such intriguing example because of the dynamic thioester bonds in their backbones, which are more reactive than their oxoester analogues.[35–47] However, PTEs are significantly less explored than polyesters due to a lack of controlled ring-opening polymerization (ROP) methods that convert thiolactones to high-molar-mass ($M_n$) polymers with narrow dispersity ($Đ$). A few recent advances by the Bowman,[37] Lu,[40] and Gutekunst[39] groups achieved modest-to-good control of PTEs, but the recycling of the polymers were not investigated. The use of amino acid as the feedstock is a smart approach to access chiral and semicrystalline polymers. We have recently reported the controlled synthesis of PTEs from 4-hydroxyproline-derived thiolactone (ProTL) monomers and demonstrated that the polymers can be conveniently depolymerized.[48] Nevertheless, these polymers are found to be brittle due to their prolyl backbone with relatively restricted conformations, necessitating further optimization of appropriate side chain and new backbone design.[49]

An interesting study by Suzuki and coworkers reported the synthesis of PTEs from a cysteine-derived β-thiolactone (CysPTE).[50] Unfortunately, the resulting polymers are characterized by relatively low molar mass (typical $M_n$ < 10 kg/mol), broad dispersity ($Đ \sim$ 1.6–2.4), and mixed linear and cyclic topologies. The underlying challenges include undesirable chain transfer, reshuffling, and backbiting, all or at least partially attributable to the extensive transthioesterification side reactions. CysPTEs are also difficult to depolymerize for monomer recycling owing to the highly strained 4-membered β-thiolactone ring. One classical strategy of accelerating ring closure and stabilizing strained rings in physical organic chemistry is the *gem*-disubstituent effect, so called Thorpe-Ingold effect.[51,52] We thus hypothesize that the introduction of a geminal dimethyl (*gem*-DM) group on the four-membered ring could tune the thermodynamics to near equilibrium for improved propensity of depolymerization, and in the meantime mitigate the reactivity of both the chain ends and PTE backbone for reduced transthioesterification (Scheme 1). Notably, such monomers can be easily produced and tailored with various side chains starting from a naturally occurring amino acid, D-penicillamine.[53,54]

## RESULTS

### Controlled Polymerization

We first synthesized five penicillamine-derived β-thiolactone monomers ($N^R$-PenTL) with different side-chains (Scheme 1B), including $N^{Ac}$-PenTL and $N^{Boc}$-PenTL as white crystals, as well as $N^{C8}$-PenTL, $N^{ene}$-PenTL, and $N^{EG4}$-PenTL as colorless oils ($^1$H and $^{13}$C NMR, high-resolution mass spectrometry, and X-ray diffraction in Figures S1–S16). Notably, the monomer synthesis is a simple and robust one-pot process and can be easily scaled up to ten-gram scale per batch in the laboratory. The ROP of each substrate was then initiated by benzyl mercaptan and catalyzed by an organobase of suitable basicity (Scheme 1B). No ROP of $N^{Ac}$-PenTL or $N^{Boc}$-PenTL was observed (Table 1, entries 1 and 2), most likely because of their limited solubility (less than ∼90 mg/mL in tetrahydrofuran [THF]), which is lower

[1]Beijing National Laboratory for Molecular Sciences, Center for Soft Matter Science and Engineering, Key Laboratory of Polymer Chemistry and Physics of Ministry of Education, College of Chemistry and Molecular Engineering, Peking University, Beijing 100871, People's Republic of China

[2]Institute of Theoretical and Computational Chemistry, Biodynamic Optical Imaging Center, College of Chemistry and Molecular Engineering, Peking University, Beijing 100871, People's Republic of China

[3]Lead Contact

*Correspondence: eqchen@pku.edu.cn (E.-Q.C.), chemhualu@pku.edu.cn (H.L.)

https://doi.org/10.1016/j.chempr.2020.06.003

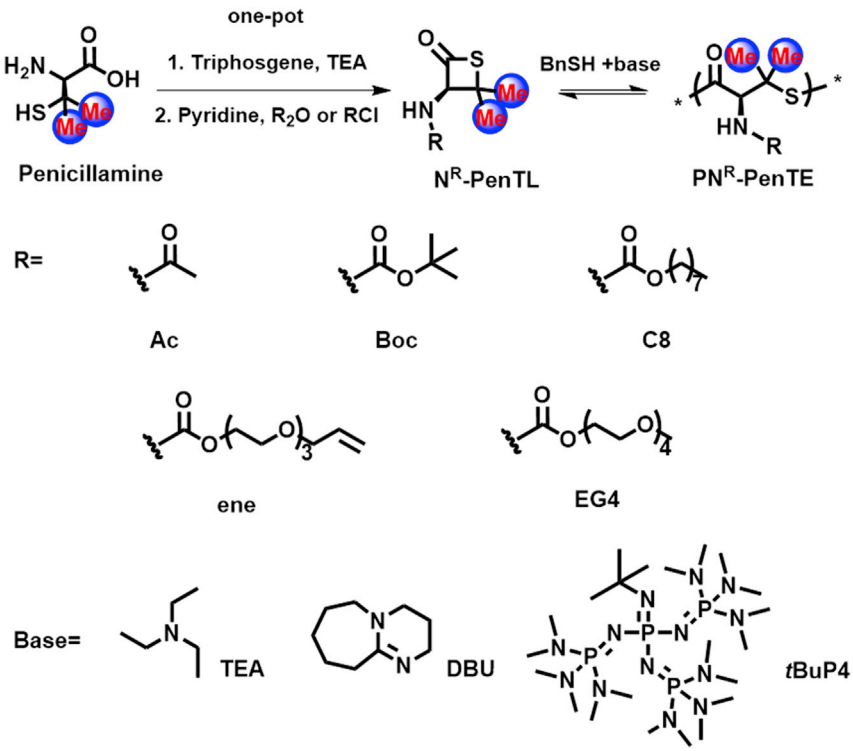


**Scheme 1. Synthesis and Ring-Opening Polymerization of Various $N^{ene}$-PenTL**

than the equilibrium monomer concentration. We therefore focused our effort on the ROP of the three liquid monomers because they were substantially more soluble in common organic solvents or could be even executed for bulk polymerization. We measured the $[M]_{eq}$ of $N^{ene}$-PenTL at various temperatures to draw the Van't Hoff plot (Figure S17). According to the linear regression, the enthalpy ($\Delta H_P^\circ$) and entropy ($\Delta S_P^\circ$) changes of the ROP were calculated to be −9.4 kJ $mol^{-1}$ and −28.1 J $mol^{-1}$ $K^{-1}$, respectively. This, in turn, gave a $\Delta G_P^\circ$ of −1.0 kJ $mol^{-1}$ (−0.24 kcal $mol^{-1}$) at 25°C and a ceiling temperature ($T_c$) of 61°C at an initial monomer concentration ($[M]_0$) of 1.0 M.

To increase reaction efficiency, we conducted bulk polymerization of $N^{ene}$-PenTL and $N^{C8}$-PenTL at room temperature and a feeding monomer/initiator ratio (M/I) of 100/1. To our gratification, the ROP of $N^{ene}$-PenTL, catalyzed by a weak organobase, triethylamine (TEA, $pK_a^{DMSO}$ = 9.0),[55] afforded the desired polymer product $PN^{ene}$-PenTE ($^1$H NMR in Figure S18) with a considerably larger $M_n$ and narrower dispersity (entry 3, Table 1; $M_n$ = 19.4 kg/mol, $Đ \sim 1.10$) than those of similar PTEs synthesized previously from CysTLs ($M_n$ ~8.8 kg/mol, $Đ \sim 2.4$) at the same M/I ratio.[50] Replacing TEA (1.0 equiv relative to initiator) with 1,8-diazabicyclo(5.4.0)undec-7-ene (DBU, 0.1 equiv), a stronger base with a $pK_a^{DMSO}$ of 12,[55] greatly accelerated the ROP reaction (Table 1, entries 4–7; Figure 1A) while preserving the controllability, as evidenced by the unimodal peaks in size-exclusion chromatography (SEC) analysis. Increasing the M/I ratio resulted in a corresponding linear elevation in the $M_n$ of $PN^{ene}$-PenTE (Figure 1A). The DBU-catalyzed ROP of $N^{ene}$-PenTL also demonstrated other typical features of controlled polymerization, such as the observation that the monomer conversion displayed a linear relationship with $M_n$ (Figure 1B). The ROP of $N^{C8}$-PenTL showed very similar controllability to that of $N^{ene}$-

**Table 1. Ring-Opening Polymerization of $N^R$-PenTL**

| Entry | Monomer | Base | $[M]_0/[I]_0/[Base]_0$ | Time (h) | $M_n^{cal}$ (g mol$^{-1}$)[a] | $M_n^{obt}$ (g mol$^{-1}$)[b] | $Đ$[c] | Conv.[d] |
|---|---|---|---|---|---|---|---|---|
| 1 | $N^{Ac}$-PenTL | TEA | 50/1/1 | 24 | 8,700 | – | – | 0 |
| 2 | $N^{Boc}$-PenTL | TEA | 50/1/1 | 24 | 11,600 | – | – | 0 |
| 3 | $N^{ene}$-PenTL | TEA | 100/1/1 | 72 | 34,700 | 19,400 | 1.10 | 61% |
| 4 | $N^{ene}$ -PenTL | DBU | 30/1/0.1 | 1 | 10,400 | 6,400 | 1.11 | 58% |
| 5 | $N^{ene}$ -PenTL | DBU | 50/1/0.1 | 3 | 17,400 | 9,900 | 1.09 | 60% |
| 6 | $N^{ene}$ -PenTL | DBU | 75/1/0.1 | 4.5 | 26,000 | 13,700 | 1.15 | 61% |
| 7 | $N^{ene}$ -PenTL | DBU | 100/1/0.1 | 6 | 34,700 | 18,500 | 1.14 | 59% |
| 8 | $N^{C8}$-PenTL | DBU | 100/1/1 | 0.3 | 28,700 | 20,100 | 1.21 | 70% |
| 9 | $N^{C8}$-PenTL | *t*BuP4 | 250/1/1 | 20 | 71,800 | 52,400 | 1.26 | 69% |
| 10 | $N^{C8}$-PenTL | *t*BuP4 | 350/1/1 | 24 | 100,500 | 70,600 | 1.23 | 70% |
| 11 | $N^{Boc}$ -PenTL, $N^{C8}$-PenTL | DBU | 30/70/0.5/1 | 1 | 27,000 | 14,100 | 1.24 | 42%, 56% |
| 12 | $N^{EG4}$-PenTL | DBU | 50/1/1 | 6 | 18,300 | 13,900 | 1.30 | 57% |

Polymerizations were initiated with benzyl mercaptan in a glovebox at room temperature. All entries were performed as bulk polymerizations except for entries 1 and 2, which were conducted in THF.

[a] $M_n^{cal}$ = calculated number-average molar mass based on the feeding M/I ratio.

[b] $M_n^{obt}$ = obtained number-average molar mass determined by SEC in DMF with 0.1 M LiBr.

[c] $Đ$ = dispersity.

[d] Monomer conversion, determined by $^1$H NMR spectroscopy.

PenTL (Table 1, entries 8–10). For example, DBU-catalyzed formation of $PN^{C8}$-PenTE ($^1$H NMR in Figure S19) at a M/I ratio of 100/1 exhibited a $M_n$ of 20.1 kg/mol and $Đ$ of 1.21 (Table 1, entry 8). Employing *t*BuP4, a phosphazene superbase with a $pK_a^{DMSO}$ of 30.3,[55] further boosted the $M_n$ to 52.4 and 70.6 kg/mol at a M/I ratio of 250/1 and 350/1, respectively, while maintaining a $Đ$ less than 1.30 (Table 1, entries 9 and 10). Copolymerization of $N^{C8}$-PenTL and $N^{Boc}$-PenTL mixture gave a random copolymer with a $M_n$ of 14.1 kg/mol and a $Đ$ ~1.24 (Table 1, entry 11). The ROP of $N^{EG4}$-PenTL, a monomer containing an oligoethyleneglycol side chain, afforded a PEG-like polymer $PN^{EG4}$-PenTE ($^1$H NMR in Figure S20) also with satisfactory control (Table 1, entry 12). Notably, all polymerizations became viscuous immediately after the addition of base and gelized eventually as a result of the high concentration. It is also noteworthy that the polymerizations needed to be carefully quenched before subsequent processing because of the reversibility.

## Facile Functionalization

Next, we examined the chain-end group of the resulting $PN^{ene}$-PenTE and its ability to undergo post-polymerization modification. Matrix-assisted laser desorption ionization-time of flight (MALDI-TOF) mass spectrum of benzyl mercaptan-initiated $PN^{ene}$-$PenTE_{15}$ contained only one set of molecular ion peaks with a spacing of 347 Da between two adjacent peaks, which corresponded to the molar mass of the monomer (Figure 1C). Moreover, the end groups were unambiguously assigned to the initiating $PhCH_2S$– group on the α end and free tertiary thiol on the ω terminus (Figure 1C, plus $Na^+$ or $K^+$). When the ROP was quenched with a small molecular capping agent, such as iodoacetamide, MALDI-TOF analysis gave exclusively $PN^{ene}$-PenTE bearing $PhCH_2S$– and $–CH_2CONH_2$ as the α and ω end groups, respectively (Figure S21). Similarly, $PN^{C8}$-PenTE also gave well-defined chain end groups in the MALDI-TOF analysis (Figures S22 and S23). Moreover, $PN^{ene}$-PenTE (ω end capped) was found to withstand typical UV-triggered thiol-ene reactions, and the side chain alkenes were converted to long alkyls (Figure S24) or anionic sulfate

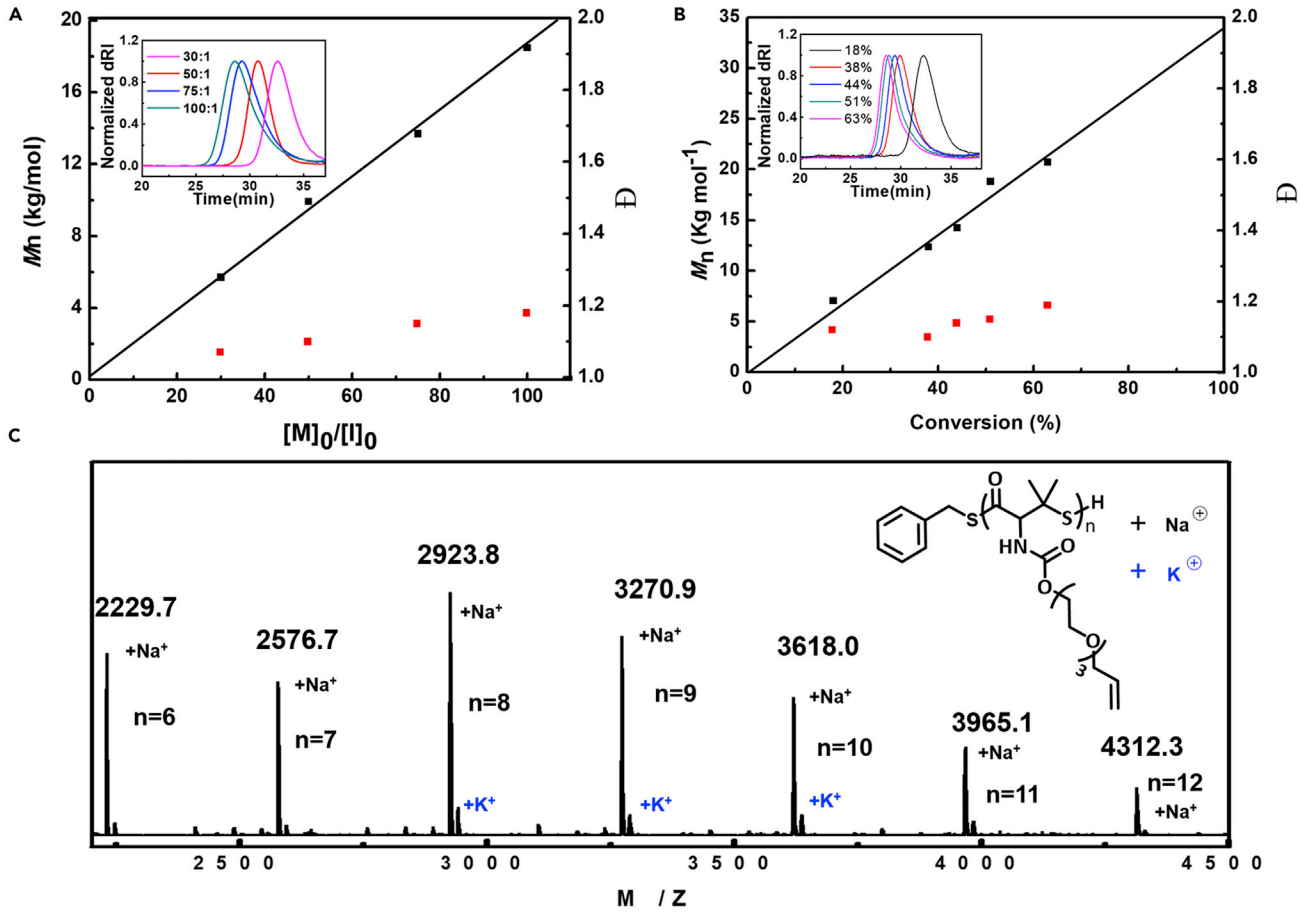


**Figure 1. Bulk ROP of Benzyl-Mercaptan-Mediated and DBU-Catalyzed $N^{ene}$-PenTL**

(A) Plots of $M_n$ and $Đ$ as a function of the $[M]_0/[I]$ ratio. Inset: overlay of SEC curves at different $[M]_0/[I]$ ratios.

(B) Plots of $M_n$ and $Đ$ as a function of monomer conversion at the $[M]_0/[I]$ ratio of 100/1. Inset: overlay of SEC curves at different monomer conversions.

(C) MALDI-TOF mass spectrum of benzyl-mercaptan-initiated $PN^{ene}$-$PenTE_{15}$.

(Figure S25) groups almost quantitatively. Together, these results indicate that not only the chain ends but also the side chain groups are easily tunable, allowing facile introduction of a variety of functionalities.

## Thermal and Mechanical Properties

Next, we studied the thermal properties of $PN^{C8}$-PenTE ($M_n$ ~70.6 kg/mol) via thermogravimetric analysis (TGA) and differential scanning calorimetry (DSC). $PN^{C8}$-PenTE showed a 5%-weight-loss decomposition temperature ($T_d$) of ~192°C regardless of the capping status at the ω end (Figure S27). DSC depicted a weak glass transition at ~50°C ($T_g$), and a large endotherm peaked at ~100°C, which corresponds to crystal melting in the heating scan (Figure 2A). Upon cooling, an exothermic peak was observed at a temperature slightly lower than the melting temperature ($T_m$). Dilatometry testing suggested that the $T_g$ and $T_m$ of the same polymer were ~45°C and ~100°C (Figure S28), respectively, which agreed well with the DSC results. In the tensile test using dynamic mechanical analysis (DMA), $PN^{C8}$-PenTE showed a Young's modulus of 300 MPa at 30°C and a catastrophic facture before yielding with a strain of 2.8% (Figure 2B). Above $T_g$, the Young's modulus reduced to 110 Mpa, and on the other hand, the breaking strain increased to 170% at 60°C

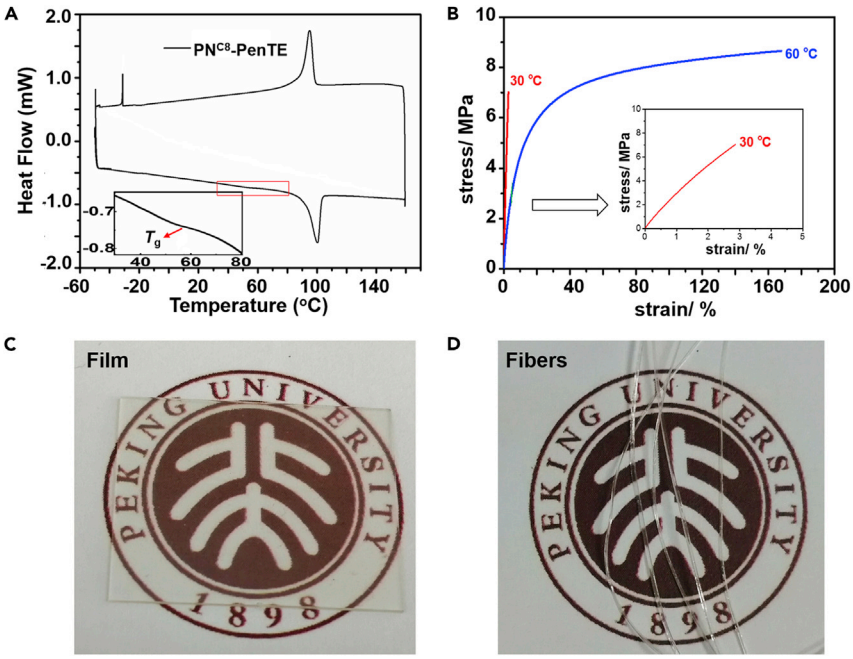


**Figure 2. Thermal and Mechanical Properties of PN$^{C8}$-PenTE Materials**

(A) DSC curve of PN$^{C8}$-PenTE.

(B) Stress-strain curves of PN$^{C8}$-PenTE test by DMA using a constant force rate of 0.5 N/min at 30°C (red) or 60°C (blue).

(C and D) Photographs of PN$^{C8}$-PenTE as a transparent film (C) and fibers (D) obtained by hot compression and melting drawing at 140°C, respectively.

(Figure 2B). PN$^{C8}$-PenTE can be manufactured into a transparent film by hot compression or flexible fibers by melt drawing at 140°C with no detectable decomposition (Figures 2C and 2D).

## Controlled and Complete Depolymerization

To investigate the depolymerization of the ω-end-uncapped PN$^{C8}$-PenTE, we tested all reactions in diluted $CDCl_3$ (initial polymer concentration = 5.0 mg/mL) by employing various bases and temperatures. When PN$^{C8}$-PenTE was mixed with 0.05 equiv DBU (relative to the number of polymer chains) at 65°C, the gradual regeneration of N$^{C8}$-PenTL was confirmed by $^1$H NMR spectroscopy and SEC. The conversion of depolymerization exhibited an inverse linear relationship with the remaining $M_n$ of the polymer (Figure 3B). Moreover, only unimodal peaks were observed in the SEC analysis of the depolymerization of PN$^{C8}$-PenTE, implying that no oligomerization occurred (Figure 3C). Meanwhile, as shown in Figure S29, the DBU (0.5 equiv)-mediated depolymerization of PN$^{C8}$-PenTE (degree of polymerization ~ 40) at room temperature gave a linear correlation of the conversion as a function of time (zero order kinetics). All these data offer convincing evidence for a domino-like unzipping depolymerization process. However, $[\alpha]_D$ testing of the 65°C recycled monomer indicated racemization (Table 2, entries 1 and 2). Interestingly, at reduced temperatures such as 25°C, PN$^{C8}$-PenTE$_{40}$ was completely depolymerized (>95%) into enantiopure monomers (Figure 3D; Table 2, entry 3) within 4 h, catalyzed by 0.1 equiv DBU. Thus, it appears that lower temperature could prevent racemization effectively. This notion was further confirmed by the fact that complete depolymerization without racemization of PN$^{C8}$-PenTE$_{40}$ was achievable within 10 min with 1 equiv DBU at −25°C (Table 2, entry 4). PN$^{ene}$-PenTE showed a very similar result

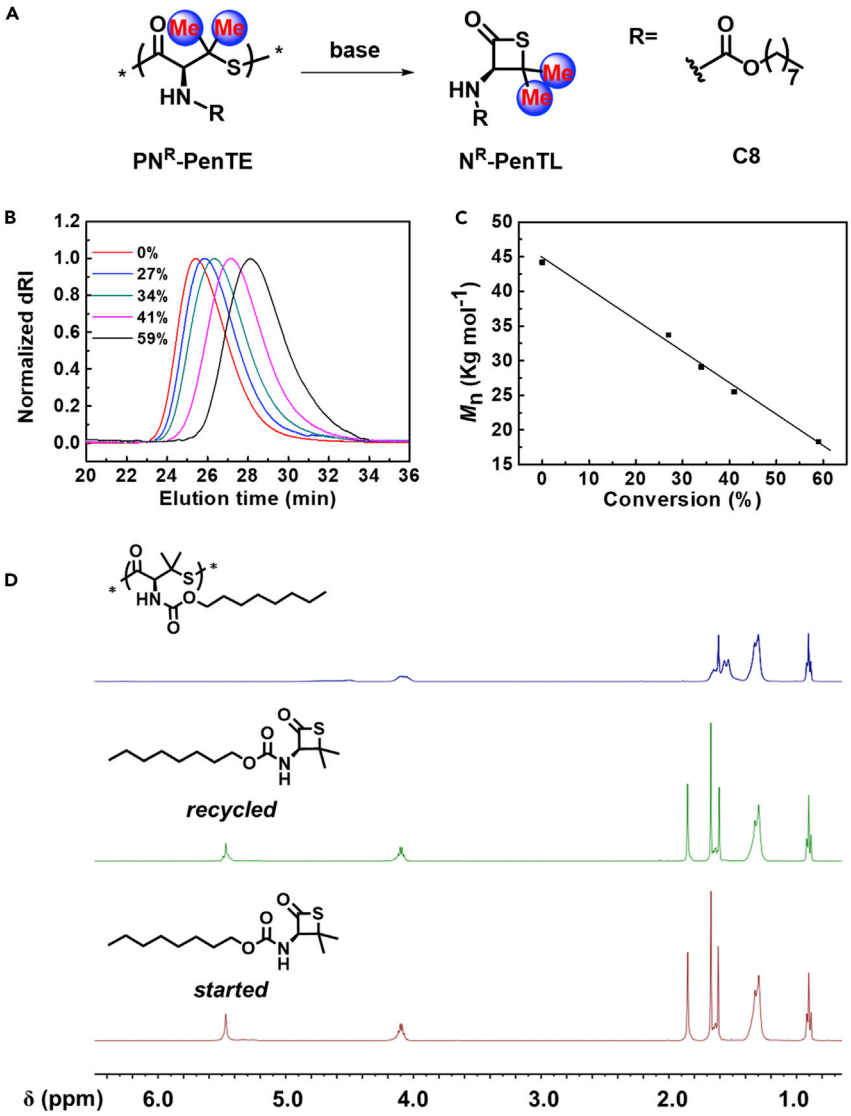


**Figure 3. DBU-Catalyzed Depolymerization of PN$^{C8}$-PenTE**

(A) Scheme of PN$^{C8}$-PenTE depolymerization.

(B) Overlay of SEC curves at different depolymerization conversions.

(C) Plot of the remaining $M_n$ of PN$^{C8}$-PenTE as a function of the conversion of the depolymerization.

(D) Overlay of the $^1$H NMR spectra in $CDCl_3$ of PN$^{C8}$-PenTE$_{40}$ (top), recycled N $^{C8}$-PenTL after depolymerization (middle), and the started N$^{C8}$-PenTL as a reference (bottom).

to PN$^{C8}$-PenTE in depolymerization (Table 2, entries 5 and 6; Figure S30). Of note, the ω-end-capped PN$^{ene}$-PenTE remained almost unchanged when mixed with 0.1 equiv DBU at 25°C for 12 h (Figure S31). The depolymerization could also be catalyzed by 1.0 equiv sodium thiophenolate (PhSNa), a weaker base but stronger nucleophile than DBU, which gave >95% conversion in less than 2 h at ambient temperature, again with no detectable racemization (Table 2, entry 5). More interestingly, even the ω-end-capped PN$^{C8}$-PenTE could be completely depolymerized when treated with 1.0 equiv PhSNa at room temperature (Figure S32), implying a complementary (mechanistic) approach to the previously described DBU-catalyzed depolymerization (Figure S33).

**Table 2. Depolymerization of $PN^{R}$-PenTE in Dilute Solution**

| Entry | Monomer or Polymer | Catalyst | Equivalents[a] | Time (min) | Temperature (°C) | $[\alpha]_D^{17.2}$[b] |
|---|---|---|---|---|---|---|
| 1 | $N^{C8}$-PenTL | – | – | – | – | −35.8 |
| 2 | $PN^{C8}$-PenTE | DBU | 0.05 | 1 | 65 | 0 |
| 3 | $PN^{C8}$-PenTE | DBU | 0.1 | 240 | 25 | −34.2 |
| 4 | $PN^{C8}$-PenTE | DBU | 1 | 10 | −25 | −35.8 |
| 5 | $PN^{C8}$-PenTE | PhSNa | 1 | 120 | 25 | −35.6 |
| 6 | $N^{ene}$-PenTL | – | – | – | – | −37.4 |
| 7 | $PN^{ene}$-PenTE | DBU | 0.1 | 240 | 25 | −36.6 |

All entries were conducted in THF at a concentration of 5.0 mg/mL.
[a]Relative to the number of polymer chains.
[b]Specific optical rotation, determined by polarimeter in THF at 17.2°C.

## Mechanism of ROP and Depolymerization

We further studied the ROP and depolymerization of $N^{R}$-PenTL by density functional theory (DFT) calculation and molecular dynamics (MD) simulation. To simplify the calculation, we used $N^{Ac}$-PenTL as a model monomer and considered the reactive chain end to consist of a dissociated anionic thiolate. The free energies of key intermediates (INTs) and transition states (TSs) in both the chain propagation and chain transfer are summarized in Figure 4A. The change in free energy of the ROP was calculated to be 0.8 kcal/mol ($INT_1$ to $INT_2$), agreeing well with the previous Van't Hoff plot (−0.24 kcal/mol). The energy barrier for the chain propagation ($INT_1$ to $TS_1$) and chain transfer ($INT_1$ to $2TS_1$) was 6.6 and 19.2 kcal/mol, respectively (Figure 4B). The ~12.6 kcal/mol difference in energy barrier, according to the Eyring equation, suggested that the rate constants of the two pathways differed from each other by an order of magnitude of ~6, which ensured that the ROP would proceed in a highly controlled fashion as we observed. Interestingly, the energy barrier of chain propagation and chain transfer in the ROP of $N^{Ac}$-CysTE were substantially lower, 0.5 and 2.2 kcal/mol, respectively (Figure S34). Such low energy barriers suggest that the rate of both propagation and transfer reactions was fast and that it was difficult to minimize chain transfer.

For depolymerization of $PN^{Ac}$-PenTE, the energy barrier was 5.8 kcal/mol ($INT_2$ to $TS_1$; Figure 4B), which served as a key contributor to the amenability of $PN^{R}$-PenTE to depolymerization. On the other hand, for $N^{Ac}$-CysTE, the change in free energy was favored for the ROP (–14.4 kcal/mol), making the reverse depolymerization pathway highly unfavorable thermodynamically (C-$INT_2$ to C-$TS_1$; Figure S34). DFT calculation further suggested that in the low-energy conformation of $PN^{R}$-PenTE, the terminal tertiary thiolate and the adjacent thioester took a gauche conformation with a S–C=O distance of ~2.96 Å and a S–C–C–CO dihedral angle ($\Psi$) of 66.4° (Figure 4C), which required no extra rotary energy for the ring-closing depolymerization. On the contrary, the low-energy conformation of $N^{Ac}$-CysTE was the staggered conformation in which the same S—C=O distance was ~4.17 Å (Figure 4C). All-atom MD simulation (Figures 4D ansd 4E) of the 20-mer of $PN^{Me}$-PenTE also suggested that the most populated conformation ($\Psi$ = 67.7%) is characterized by an average S–C=O distance of 3.4 Å between the terminal thiol and its adjacent thioester carbon, whereas the staggered conformations with a longer distance (4.20 Å in average) were less populated (18.2%). This restrained conformation is a clear indication of the Thorpe-Ingold effect induced by the *gem*-DM.[51,52]

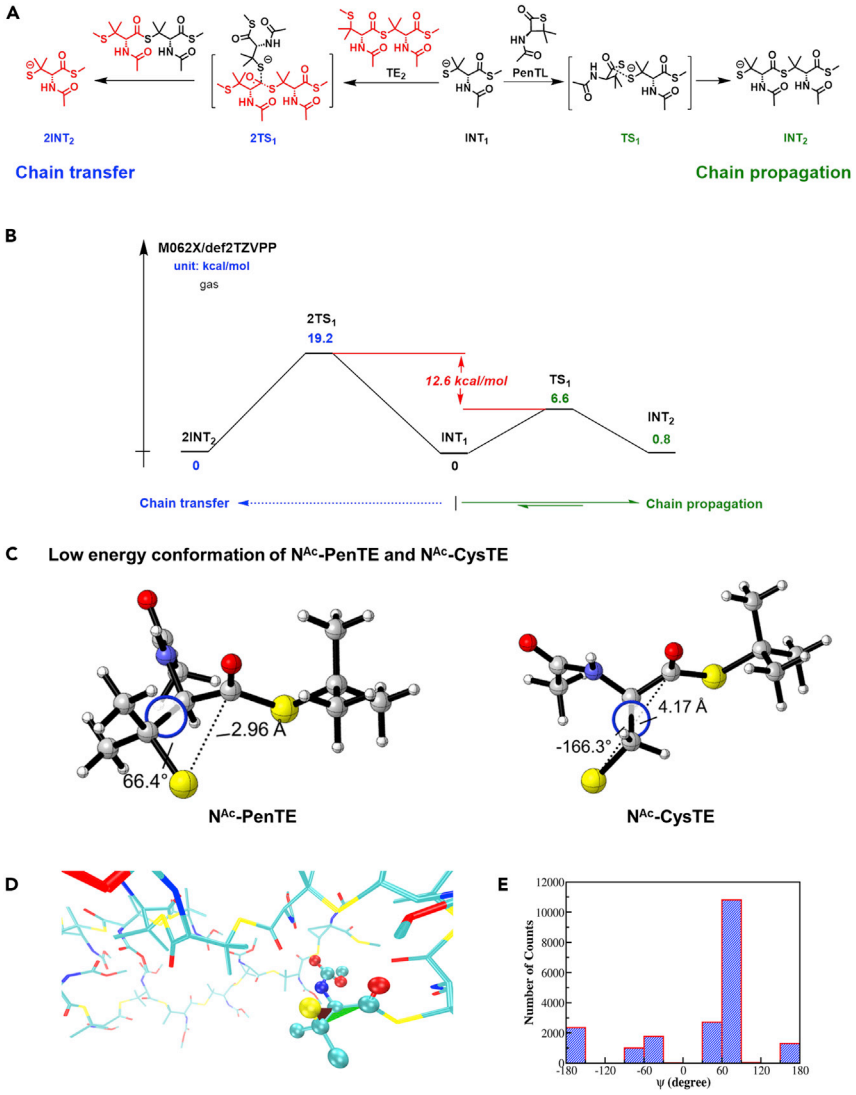


**Figure 4. Mechanistic Investigation of the ROP and Chain Transfer by DFT Calculation and MD Simulation**

(A) Proposed chain propagation and transfer intermediates (INTs) and transition states (TSs) in the ROP of $N^{R}$-PenTL in gas.

(B) Calculated free energy of each INT and TS.

(C) Low-energy conformation of $N^{A}$-PenTE and $N^{Ac}$-CysTE.

(D) The most popular conformation of PNMe-$PenTE_{20}$.

(E) Ψ dihedral angle distribution of different conformations of $PN^{Me}$-$PenTE_{20}$.

## DISCUSSION

The unique thermomechanical, optical, and dynamic properties of PTE polymers, coupled with a global emphasis on environmental sustainability, have propelled a resurgence in their popularity.[35,56,57] Although chemical production[47] and biosynthesis[58] of PTEs were first reported in 1968 and 2001, respectively, controlled chemical synthesis of high $M_n$ PTEs remains a technological bottleneck because of the dynamic nature of thioesters. In this work, we achieved the controlled ROP of β-thiolactones by introducing a *gem*-DM group on the four-membered ring (Figure 1; Table 1). The facile access to high $M_n$ PTEs under mild conditions could provide a significant boost to their industrial and biomedical application.

Functionalization of both the termini and side groups in $PN^{R}$-PenTE opens up opportunities to create novel, high-performance materials by introducing different combinations of substituents to the polymer chain. As demonstrated earlier, the *N*-octanoyloxy groups in $PN^{C8}$-PenTL confer semicrystallinity and increase processability and durability (Figure 2). On the other hand, $PN^{EG4}$-PenTE (Table 1, entry 12) exhibits excellent water solubility and degradability, making it an attractive alternative to PEG and a promising high-value biomaterial for temperature-induced self-assembly and/or therapeutic protein conjugation.[59,60] The physicochemical properties of $PN^{R}$-PenTE could be further expanded or fine-tuned by copolymerizing several types of monomers with different side chains (Table 1, entry 11).

Previously reported strategies for polymer recycling predominantly involved reverting back to cyclic monomers bearing a five- or six-membered ring, which are relatively unstrained.[17,19,22,31,61] We recently succeeded in extending the scope of such regenerative building blocks to bridged bicyclic thiolactones.[48] In the current study, we further demonstrated, on the basis of both experimental data and theoretical calculations, that the presence of *gem*-DM played a key role in enabling fast, selective, and highly controlled depolymerization of $PN^{R}$-PenTEs (Figures 3 and 4). Of note, although depolymerizable polymers were not uncommon, the domino-like unzipping fashion in the depolymerization of $PN^{R}$-PenTEs without the generation of thermodynamic equilibrium mixture of oligomeric intermediates (Figures 3A, 3B, and S29) was relatively rare. This control was again most likely empowered by the presence of *gem*-DM (Figures 4C–4E). It is also worth pointing out that similar ring-closure reactions that are driven by the Thorpe-Ingold effect have been frequently employed.[62–64] Thus, we envisage that our current strategy can be broadly applied to the design of various recyclable polymers beyond $PN^{R}$-PenTEs. The PhSNa-mediated complete depolymerization of both ω-end-capped and -uncapped $PN^{R}$-PenTEs allows more versatile end-group functionalization without jeopardizing the recycling capability of PTEs and thus opens new opportunities to a broader scope of applications.

It should be noted that the relatively high price of penicillamine could pose a challenge to our method when applied on an industrial scale. Nevertheless, cost mitigation could potentially be achieved by further optimizing the chemical and/or biosynthetic-based routes to produce similar substrate monomers in a more affordable manner.[65] Overall, the strategy can be utilized to rapidly and efficiently generate a wide range of high-value, recyclable polymers with immense application potential as self-immolative materials,[66,67] covalent adaptable networks,[68] sacrificial domain for composites and nanolithography, and responsive biomaterials.[56]

## EXPERIMENTAL PROCEDURES

### Resource Availability

#### *Lead Contact*

Requests for further information should be directed to and will be fulfilled by the Lead Contact, Hua Lu (chemhualu@pku.edu.cn).

#### *Materials Availability*

This study did not generate new unique materials.

#### *Data and Code Availability*

The accession number for the crystallographic data reported in this paper is CCDC: 2004873. These data can be obtained free of charge from the Cambridge Crystallographic Data Centre at https://www.ccdc.cam.ac.uk/structures/.

The Cartesian coordinates of structures can be found in Data S1.

### General Procedure for the Ring-Opening Polymerization of $N^{R}$-PenTL

In a glovebox, benzyl mercaptan (2.0 M, 29.5 μL, 1.0 equiv) and DBU (2.0 M, 3.0 μL, 0.10 equiv) in THF were added to $N^{C8}$-PenTL (1,740 mg, 0.35 mmol, 100 equiv). The polymerization was kept at ambient temperature for 24 h. Upon reaching equilibrium, iodoacetamide (1.0 M, 300 μL, 5.0 equiv) in THF or trifluoroacetic acid (1.0 equiv) was added to quench the polymerization. The mixture was diluted with DCM (10 mL), precipitated in isopropanol (450 mL), and collected with centrifugation. The crude product was further purified by repeating the solution-precipitation-centrifugation cycle twice to obtain a white solid before drying under vacuum (920 mg, yield 53%).

Full experimental procedures are provided in the Supplemental Information.

## SUPPLEMENTAL INFORMATION

Supplemental Information can be found online at https://doi.org/10.1016/j.chempr.2020.06.003.

## ACKNOWLEDGMENTS

This work was supported by the National Natural Science Foundation of China (21722401 to H.L. and 21634001 to E.-Q.C.). Z.Y.T. was supported by the National Postdoctoral Program for Innovative Talents of China (BX20190004). The computation was supported by the High-Performance Computing Platform of Peking University. We thank Prof. Suwei Dong and Prof. Zichen Li for inspiring discussions.

## AUTHOR CONTRIBUTIONS

H.L. and W.X. conceived the project and designed the experiments. W.X., Z.T., H.W., X.Z., and Z.Z. performed synthesis. W.X., W.C., and D.S. prepared and characterized the bulk materials. W.X. conducted the DFT calculation. L.Y. performed the MD simulation. W.X., D.S., E.-Q.C., and H.L. analyzed data and wrote the manuscript. All authors approved the final version.

## DECLARATION OF INTERESTS

The authors declare no competing interests.

Received: February 28, 2020
Revised: April 30, 2020
Accepted: May 29, 2020
Published: June 22, 2020

## REFERENCES

1. Tang, X., and Chen, E.Y.-X. (2019). Toward infinitely recyclable plastics derived from renewable cyclic esters. Chem *5*, 284–312.

2. Geyer, R., Jambeck, J.R., and Law, K.L. (2017). Production, use, and fate of all plastics ever made. Sci. Adv. *3*, e1700782.

3. Jehanno, C., Flores, I., Dove, A.P., Müller, A.J., Ruipérez, F., and Sardon, H. (2018). Organocatalysed depolymerisation of Pet in a fully sustainable cycle using thermally stable protic ionic salt. Green Chem *20*, 1205–1212.

4. Jia, X.Q., Qin, C., Friedberger, T., Guan, Z.B., and Huang, Z. (2016). Efficient and selective degradation of polyethylenes into liquid fuels and waxes under mild conditions. Sci. Adv. *2*, e1501591.

5. Jehanno, C., Pérez-Madrigal, M.M., Demarteau, J., Sardon, H., and Dove, A.P. (2019). Organocatalysis for depolymerisation. Polym. Chem. *10*, 172–186.

6. Zhu, Y.Q., Romain, C., and Williams, C.K. (2016). Sustainable polymers from renewable resources. Nature *540*, 354–362.

7. Albertsson, A.C., and Hakkarainen, M. (2017). Designed to degrade. Science *358*, 872–873.

8. Garcia, J.M., and Robertson, M.L. (2017). The future of plastics recycling. Science *358*, 870–872.

9. Hillmyer, M.A. (2017). The promise of plastics from plants. Science *358*, 868–870.

10. García, J.M., Jones, G.O., Virwani, K., McCloskey, B.D., Boday, D.J., ter Huurne, G.M., Horn, H.W., Coady, D.J., Bintaleb, A.M., Alabdulrahman, A.M.S., et al. (2014).

Recyclable, strong thermosets and organogels via paraformaldehyde condensation with diamines. Science *344*, 732–735.

11. Zhang, X.Y., Fevre, M., Jones, G.O., and Waymouth, R.M. (2018). Catalysis as an enabling science for sustainable polymers. Chem. Rev. *118*, 839–885.

12. Tretbar, C.A., Neal, J.A., and Guan, Z.B. (2019). Direct silyl ether metathesis for vitrimers with exceptional thermal stability. J. Am. Chem. Soc. *141*, 16595–16599.

13. Höcker, H., and Keul, H. (1994). Ring-opening polymerization and ring-closing depolymerization. Adv. Mater. *6*, 21–36.

14. Endo, T., Kakimoto, K., Ochiai, B., and Nagai, D. (2005). Synthesis and chemical recycling of a polycarbonate obtained by anionic ring-opening polymerization of a bifunctional cyclic carbonate. Macromolecules *38*, 8177–8182.

15. Endo, T., and Nagai, D. (2005). A novel construction of ring-opening polymerization and chemical recycling system. Macromol. Symp. *226*, 79–86.

16. Olsén, P., Odelius, K., and Albertsson, A.C. (2016). Thermodynamic presynthetic considerations for ring-opening polymerization. Biomacromolecules *17*, 699–709.

17. Olsén, P., Undin, J., Odelius, K., Keul, H., and Albertsson, A.C. (2016). Switching from controlled ring-opening polymerization (crop) to controlled ring-closing depolymerization (Crcdp) by adjusting the reaction parameters that determine the ceiling temperature. Biomacromolecules *17*, 3995–4002.

18. Sangroniz, A., Zhu, J.B., Tang, X., Etxeberria, A., Chen, E.Y.X., and Sardon, H. (2019). Packaging materials with desired mechanical and barrier properties and full chemical recyclability. Nat. Commun. *10*, 3559.

19. Hong, M., and Chen, E.Y.X. (2016). Completely recyclable biopolymers with linear and cyclic topologies via ring-opening polymerization of gamma-butyrolactone. Nat. Chem. *8*, 42–49.

20. Zhu, J.B., Watson, E.M., Tang, J., and Chen, E.Y.X. (2018). A synthetic polymer system with repeatable chemical recyclability. Science *360*, 398–403.

21. Xu, S., Lamm, M.E., Rahman, M.A., Zhang, X., Zhu, T., Zhao, Z., and Tang, C. (2018). Renewable atom-efficient polyesters and thermosetting resins derived from high oleic soybean oil. Green Chem *20*, 1106–1113.

22. Liu, Y., Zhou, H., Guo, J.Z., Ren, W.M., and Lu, X.B. (2017). Completely recyclable monomers and polycarbonate: approach to sustainable polymers. Angew. Chem. Int. Ed. *56*, 4862–4866.

23. Liu, Y., and Mecking, S. (2019). A synthetic polyester from plant oil feedstock by functionalizing polymerization. Angew. Chem. Int. Ed. *58*, 3346–3350.

24. Myers, D., Witt, T., Cyriac, A., Bown, M., Mecking, S., and Williams, C.K. (2017). Ring opening polymerization of macrolactones: high conversions and activities using an yttrium catalyst. Polym. Chem. *8*, 5780–5785.

25. Song, Y., Ji, X., Dong, M., Li, R., Lin, Y.N., Wang, H., and Wooley, K.L. (2018). Advancing the development of highly-functionalizable glucose-based polycarbonates by tuning of the glass transition temperature. J. Am. Chem. Soc. *140*, 16053–16057.

26. Miyaji, H., Satoh, K., and Kamigaito, M. (2016). Bio-based polyketones by selective ring-opening radical polymerization of alpha-pinene-derived pinocarvone. Angew. Chem. Int. Ed. *55*, 1372–1376.

27. Bhaumik, A., Peterson, G.I., Kang, C., and Choi, T.L. (2019). Controlled living cascade polymerization to make fully degradable sugar-based polymers from D-glucose and D-galactose. J. Am. Chem. Soc. *141*, 12207–12211.

28. Saxon, D.J., Nasiri, M., Mandal, M., Maduskar, S., Dauenhauer, P.J., Cramer, C.J., LaPointe, A.M., and Reineke, T.M. (2019). Architectural control of isosorbide-based polyethers via ring-opening polymerization. J. Am. Chem. Soc. *141*, 5107–5111.

29. De Hoe, G.X., Zumstein, M.T., Tiegs, B.J., Brutman, J.P., McNeill, K., Sander, M., Coates, G.W., and Hillmyer, M.A. (2018). Sustainable polyester elastomers from lactones: synthesis, properties, and enzymatic hydrolyzability. J. Am. Chem. Soc. *140*, 963–973.

30. Chen, X., Chen, G., Tao, Y., Wang, Y., Lu, X.-B., Zhang, L., Zhu, J., Zhang, J., and Wang, X. (2019). Research progress in eco-polymers. Acta Polym. Sin. *50*, 1068–1082.

31. Zhao, N., Ren, C., Li, H., Li, Y., Liu, S., and Li, Z. (2017). Selective ring-opening polymerization of non-strained gamma-butyrolactone catalyzed by a cyclic trimeric phosphazene base. Angew. Chem. Int. Ed. *56*, 12987–12990.

32. Feist, J.D., and Xia, Y. (2020). Enol ethers are effective monomers for ring-opening metathesis polymerization: synthesis of degradable and depolymerizable poly(2,3-dihydrofuran). J. Am. Chem. Soc. *142*, 1186–1189.

33. Zhang, C.-J., Hu, L.-F., Wu, H.-L., Cao, X.-H., and Zhang, X.-H. (2018). Dual organocatalysts for highly active and selective synthesis of linear poly(gamma-butyrolactone)S with high molecular weights. Macromolecules *51*, 8705–8711.

34. Shen, Y., Xiong, W., Li, Y.-Z., Zhao, Z.-C., Lu, H., and Li, Z.-B. (2020). Chemoselective polymerization of fully biorenewable α-methylene-γ-butyrolactone using organophosphazene/urea binary catalysts system towards a sustainable polyesters. CCS Chem. https://doi.org/10.31635/ccschem.020.202000232.

35. Aksakal, S., Aksakal, R., and Becer, C.R. (2018). Thioester functional polymers. Polym. Chem. *9*, 4507–4516.

36. Wang, C., Mavila, S., Worrell, B.T., Xi, W.X., Goldman, T.M., and Bowman, C.N. (2018). Productive exchange of thiols and thioesters to form dynamic polythioester-based polymers. ACS Macro Lett *7*, 1312–1316.

37. Mavila, S., Worrell, B.T., Culver, H.R., Goldman, T.M., Wang, C., Lim, C.H., Domaille, D.W., Pattanayak, S., McBride, M.K., Musgrave, C.B., and Bowman, C.N. (2018). Dynamic and responsive DNA-like polymers. J. Am. Chem. Soc. *140*, 13594–13598.

38. Espeel, P., Carrette, L.L.G., Bury, K., Capenberghs, S., Martins, J.C., Du Prez, F.E., and Madder, A. (2013). Multifunctionalized sequence-defined oligomers from a single building block. Angew. Chem. Int. Ed. *52*, 13261–13264.

39. Smith, R.A., Fu, G., McAteer, O., Xu, M., and Gutekunst, W.R. (2019). Radical approach to thioester-containing polymers. J. Am. Chem. Soc. *141*, 1446–1451.

40. Yue, T.J., Zhang, M.C., Gu, G.G., Wang, L.Y., Ren, W.M., and Lu, X.B. (2019). Precise synthesis of poly(thioester)S with diverse structures by copolymerization of cyclic thioanhydrides and episulfides mediated by organic ammonium salts. Angew. Chem. Int. Ed. *58*, 618–623.

41. Bannin, T.J., and Kiesewetter, M.K. (2015). Poly(thioester) by organocatalytic ring-opening polymerization. Macromolecules *48*, 5481–5486.

42. Ura, Y., Al-Sayah, M., Montenegro, J., Beierle, J.M., Leman, L.J., and Ghadiri, M.R. (2009). Dynamic polythioesters via ring-opening polymerization of 1,4-thiazine-2,5-diones. Org. Biomol. Chem. *7*, 2878–2884.

43. Kricheldorf, H.R., and Schwarz, G. (2007). Poly(thioester)s. J. Macromol. Sci. A *44*, 625–649.

44. Ghobril, C., Charoen, K., Rodriguez, E.K., Nazarian, A., and Grinstaff, M.W. (2013). A dendritic thioester hydrogel based on thiol-thioester exchange as a dissolvable sealant system for wound closure. Angew. Chem. Int. Ed. *52*, 14070–14074.

45. Lütke-Eversloh, T., Fischer, A., Remminghorst, U., Kawada, J., Marchessault, R.H., Bögershausen, A., Kalwei, M., Eckert, H., Reichelt, R., Liu, S.J., and Steinbüchel, A. (2002). Biosynthesis of novel thermoplastic polythioesters by engineered Escherichia coli. Nat. Mater. *1*, 236–240.

46. Kato, M., Toshima, K., and Matsumura, S. (2007). Enzymatic synthesis of polythioester by the ring-opening polymerization of cyclic thioester. Biomacromolecules *8*, 3590–3596.

47. Overberger, C.G., and Weise, J.K. (1968). Anionic ring-opening polymerization of thiolactones. J. Am. Chem. Soc. *90*, 3533–3537.

48. Yuan, J., Xiong, W., Zhou, X., Zhang, Y., Shi, D., Li, Z., and Lu, H. (2019). 4-Hydroxyproline-derived sustainable polythioesters: controlled ring-opening polymerization, complete recyclability, and facile functionalization. J. Am. Chem. Soc. *141*, 4928–4935.

49. Yuan, J., Shi, D., Zhang, Y., Lu, J., Wang, L., Chen, E.-Q., and Lu, H. (2020). 4-Hydroxy-l-proline as a general platform for stereoregular aliphatic polyesters: controlled ring-opening polymerization, facile functionalization, and site-specific bioconjugation. CCS Chem *2*, 236–244.

50. Suzuki, M., Makimura, K., and Matsuoka, S. (2016). Thiol-mediated controlled ring-opening polymerization of cysteine-derived beta-thiolactone and unique features of

product polythioester. Biomacromolecules *17*, 1135–1141.

51. Jung, M.E., and Piizzi, G. (2005). Gem-disubstituent effect: theoretical basis and synthetic applications. Chem. Rev. *105*, 1735–1766.

52. Bachrach, S.M. (2008). The gem-dimethyl effect revisited. J. Org. Chem. *73*, 2466–2468.

53. Chen, H., Xiao, Y.X., Yuan, N., Weng, J.P., Gao, P.C., Breindel, L., Shekhtman, A., and Zhang, Q. (2018). Coupling of sterically demanding peptides by beta-thiolactone-mediated native chemical ligation. Chem. Sci. *9*, 1982–1988.

54. Wang, Y., Han, L., Yuan, N., Wang, H., Li, H., Liu, J., Chen, H., Zhang, Q., and Dong, S. (2018). Traceless beta-mercaptan-assisted activation of valinyl benzimidazolinones in peptide ligations. Chem. Sci. *9*, 1940–1946.

55. Tshepelevitsh, S., Kütt, A., Lõkov, M., Kaljurand, I., Saame, J., Heering, A., Plieger, P.G., Vianello, R., and Leito, I. (2019). On the basicity of organic bases in different media. Eur. J. Org. Chem. *2019*, 6735–6748.

56. Brown, T.E., Carberry, B.J., Worrell, B.T., Dudaryeva, O.Y., McBride, M.K., Bowman, C.N., and Anseth, K.S. (2018). Photopolymerized dynamic hydrogels with tunable viscoelastic properties through thioester exchange. Biomaterials *178*, 496–503.

57. Mutlu, H., Ceper, E.B., Li, X., Yang, J., Dong, W., Ozmen, M.M., and Theato, P. (2019). Sulfur chemistry in polymer and materials science. Macromol. Rapid Commun. *40*, e1800650.

58. Lütke-Eversloh, T., Bergander, K., Luftmann, H., and Steinbüchel, A. (2001). Identification of a new class of biopolymer: bacterial synthesis of a sulfur-containing polymer with thioester linkages. Microbiology (Reading Engl.) *147*, 11–19.

59. Lu, J., Wang, H., Tian, Z., Hou, Y., and Lu, H. (2020). Cryopolymerization of 1,2-dithiolanes for the facile and reversible grafting-from synthesis of protein–polydisulfide conjugates. J. Am. Chem. Soc. *142*, 1217–1221.

60. Hou, Y., and Lu, H. (2019). Protein pepylation: a new paradigm of protein–polymer conjugation. Bioconjug. Chem. *30*, 1604–1616.

61. MacDonald, J.P., and Shaver, M.P. (2016). An aromatic/aliphatic polyester prepared via ring-opening polymerisation and its remarkably selective and cyclable depolymerisation to monomer. Polym. Chem. *7*, 553–559.

62. Huang, H.C., Wang, W.Q., Zhou, Z.F., Sun, B.H., An, M.R., Haeffner, F., and Niu, J. (2019). Radical ring-closing/ring-opening cascade polymerization. J. Am. Chem. Soc. *141*, 12493–12497.

63. Gutekunst, W.R., and Hawker, C.J. (2015). A general approach to sequence-controlled polymers using macrocyclic ring opening metathesis polymerization. J. Am. Chem. Soc. *137*, 8038–8041.

64. Lee, H.K., Lee, J., Kockelmann, J., Herrmann, T., Sarif, M., and Choi, T.L. (2018). Superior cascade ring-opening/ring-closing metathesis polymerization and multiple olefin metathesis polymerization: enhancing the driving force for successful polymerization of challenging monomers. J. Am. Chem. Soc. *140*, 10536–10545.

65. Kulkarni, G.M., Kulkarni, S., and Sharma, N. (2018). A novel, feasible and cost effective process for the manufacture of D–penicillamine. Patent WO 2018/134836 A1, filed August 21, 2017, and published July 26, 2018.

66. Sagi, A., Weinstain, R., Karton, N., and Shabat, D. (2008). Self-immolative polymers. J. Am. Chem. Soc. *130*, 5434–5435.

67. Peterson, G.I., Larsen, M.B., and Boydston, A.J. (2012). Controlled depolymerization: stimuli-responsive self-immolative polymers. Macromolecules *45*, 7317–7328.

68. Bowman, C.N., and Kloxin, C.J. (2012). Covalent adaptable networks: reversible bond structures incorporated in polymer networks. Angew. Chem. Int. Ed. *51*, 4272–4274.

**Chem, Volume *6***

## Supplemental Information

# Geminal Dimethyl Substitution Enables Controlled Polymerization of Penicillamine-Derived β-Thiolactones and Reversed Depolymerization

**Wei Xiong, Wenying Chang, Dong Shi, Lijiang Yang, Ziyou Tian, Hao Wang, Zhengchu Zhang, Xuhao Zhou, Er-Qiang Chen, and Hua Lu**

**Supplemental data items**

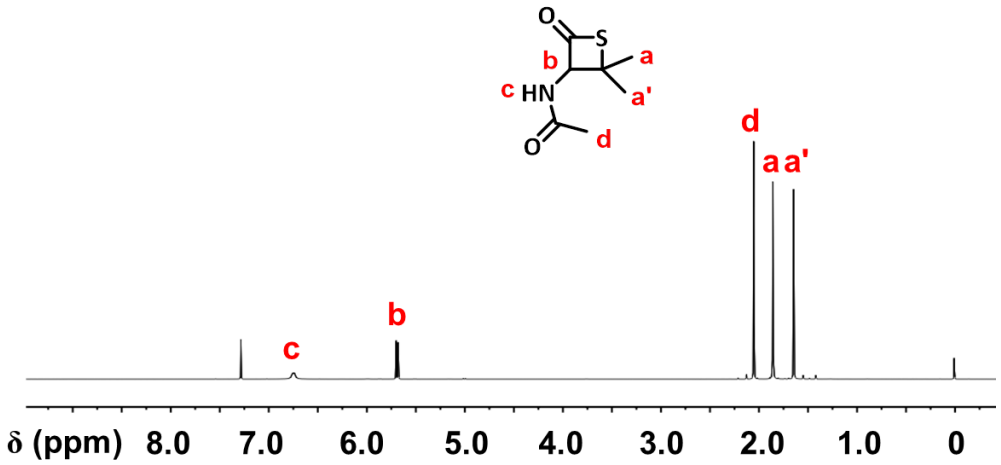


**Figure S1.** $^{1}H$ NMR spectrum of $N^{Ac}$-PenTL in $CDCl_3$.

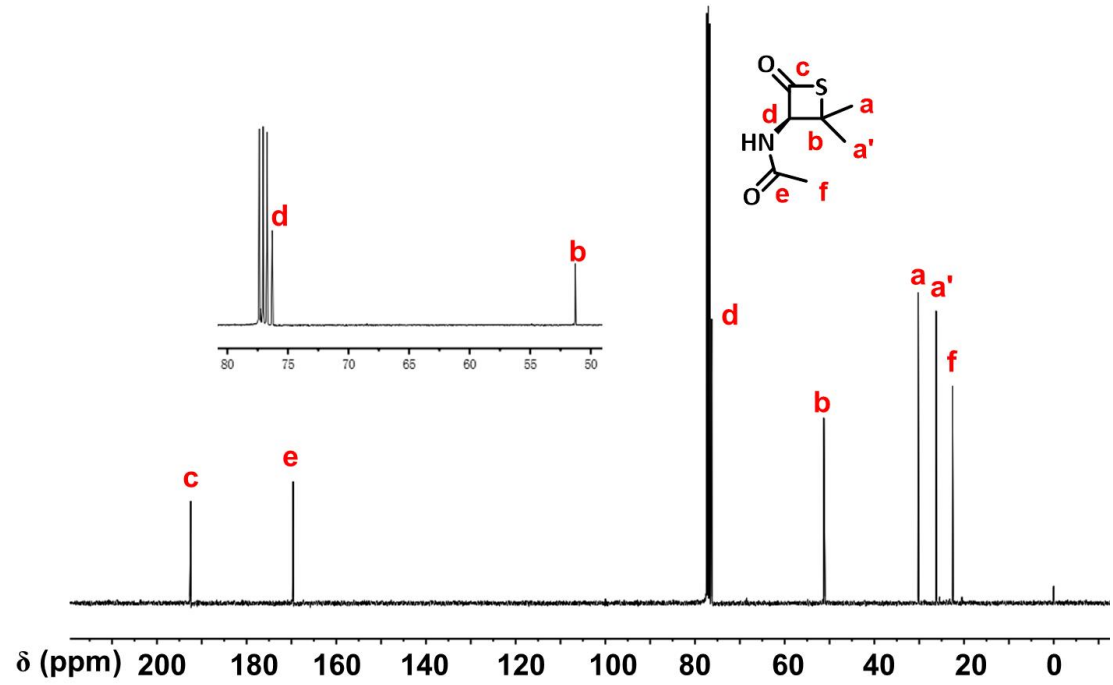


**Figure S2.** $^{13}C$ NMR spectrum of $N^{Ac}$-PenTL in $CDCl_3$.

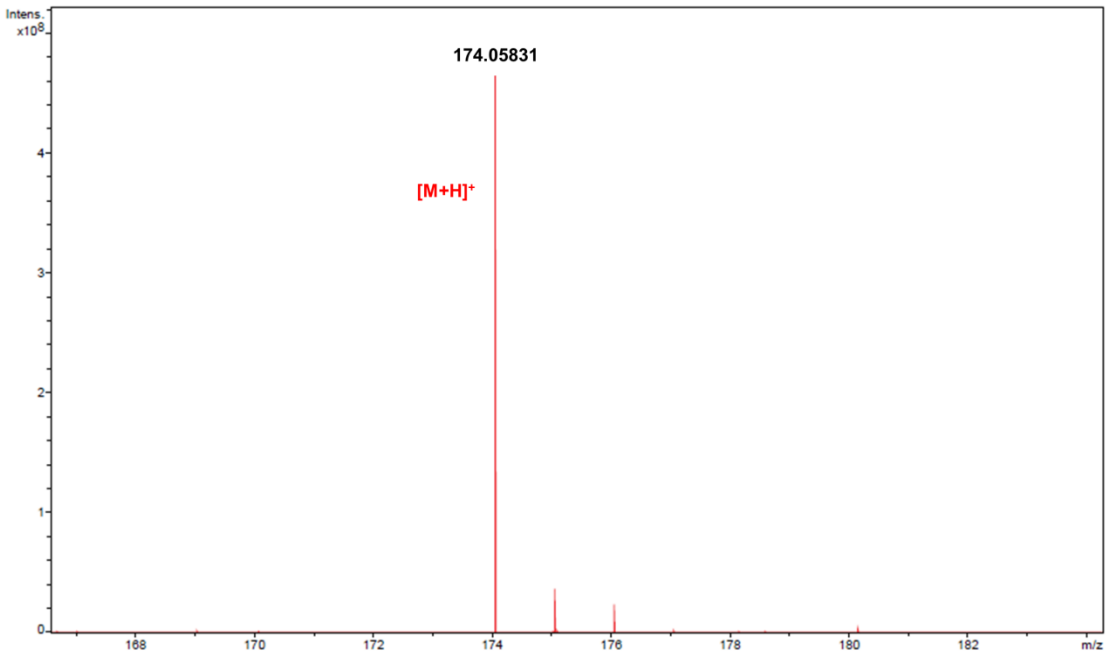


**Figure S3.** HR-MS spectrum of $N^{Ac}$-PenTL.

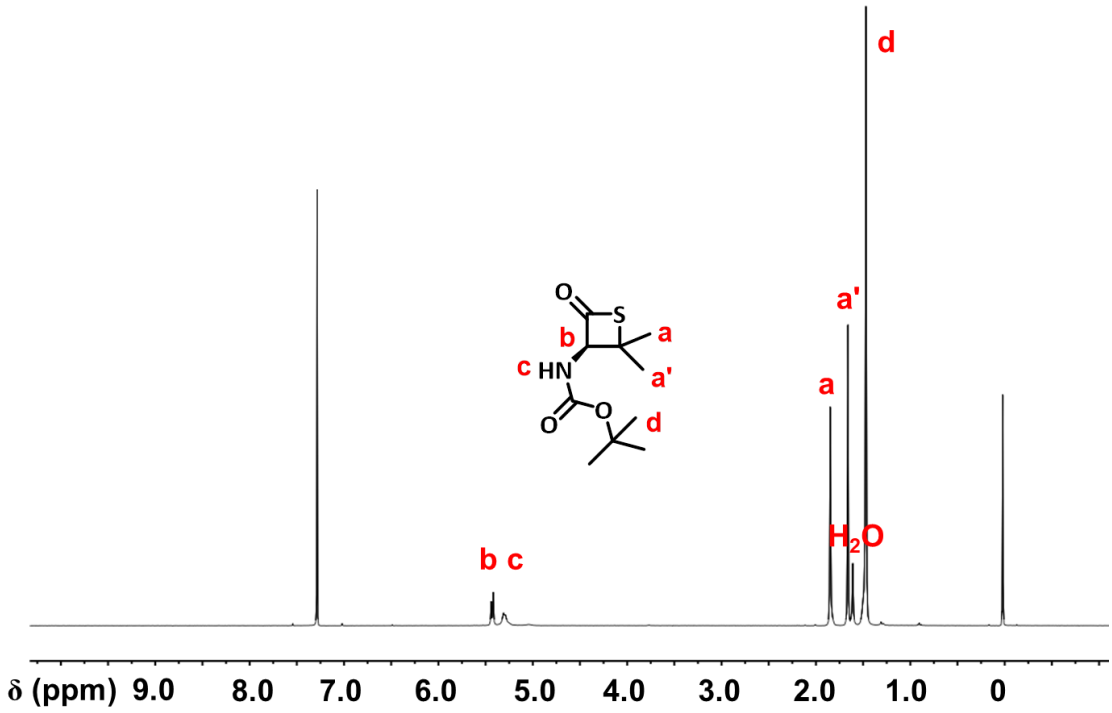


**Figure S4.** $^{1}H$ NMR spectrum of $N^{Boc}$-PenTL in $CDCl_3$.

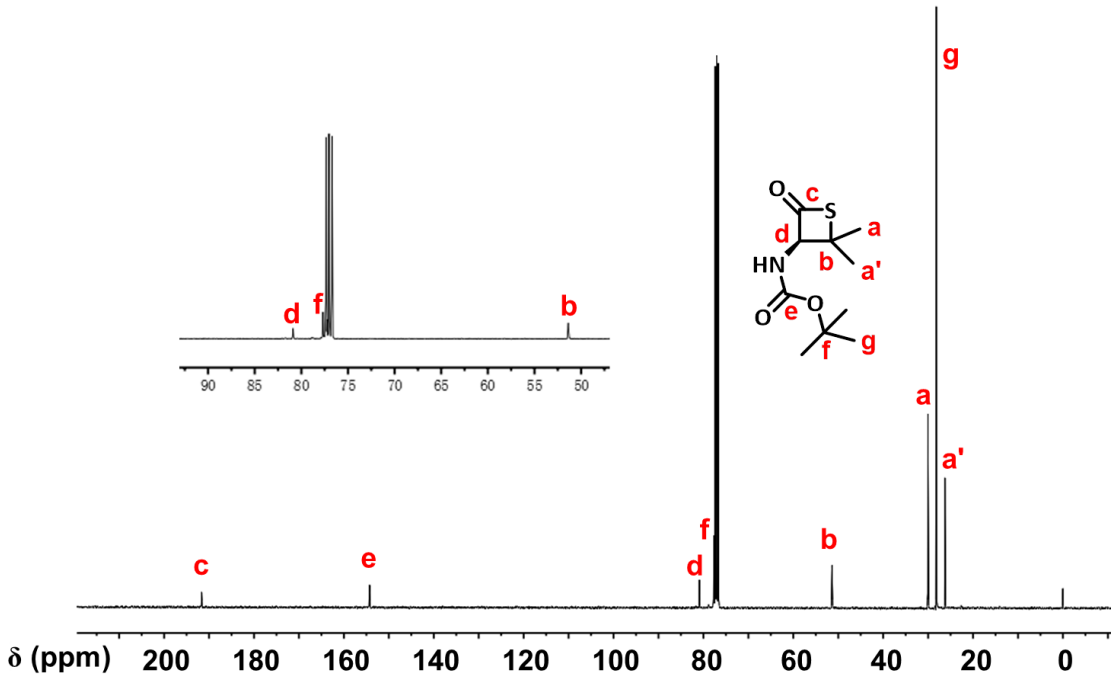


**Figure S5.** $^{13}C$ NMR spectrum of $N^{Boc}$-PenTL in $CDCl_3$.

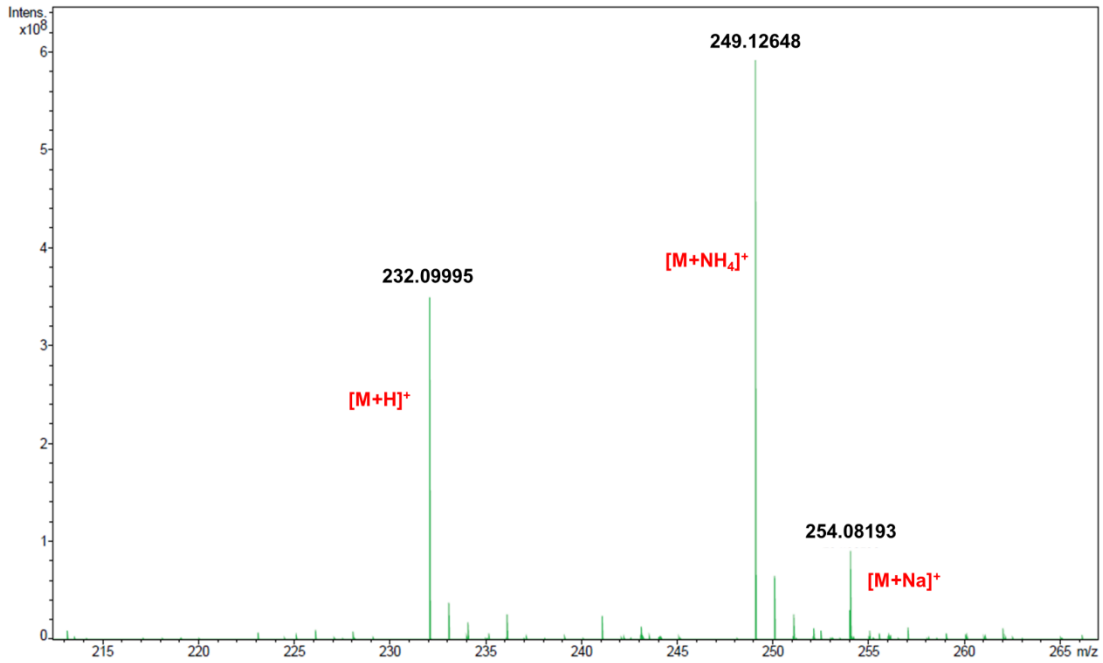


**Figure S6.** HR-MS spectrum of $N^{Boc}$-PenTL.

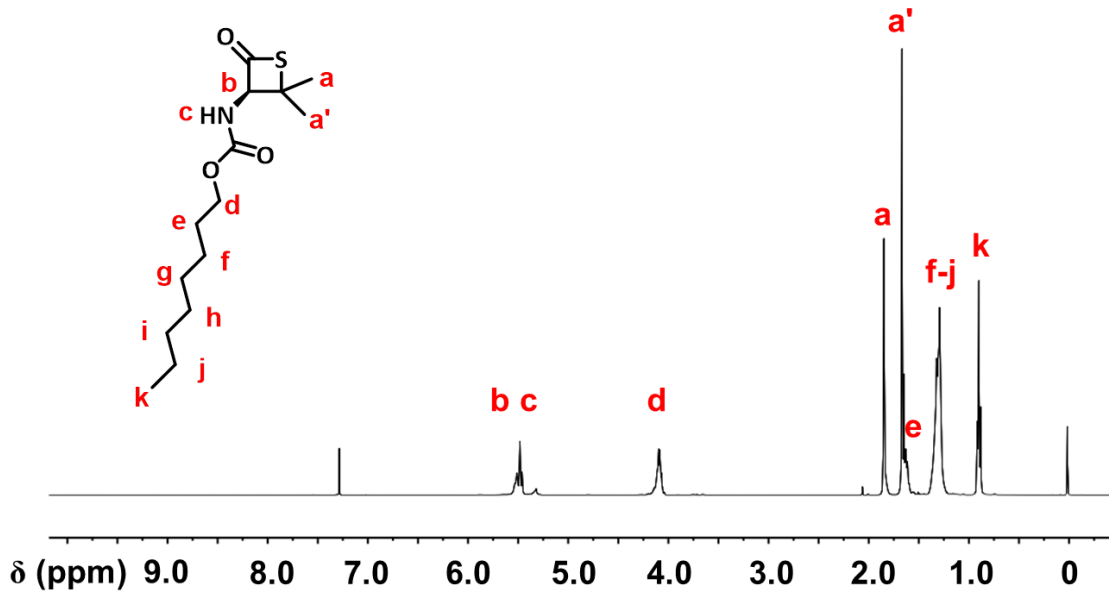


**Figure S7.** $^{1}$H NMR spectrum of N$^{C8}$-PenTL in $CDCl_3$.

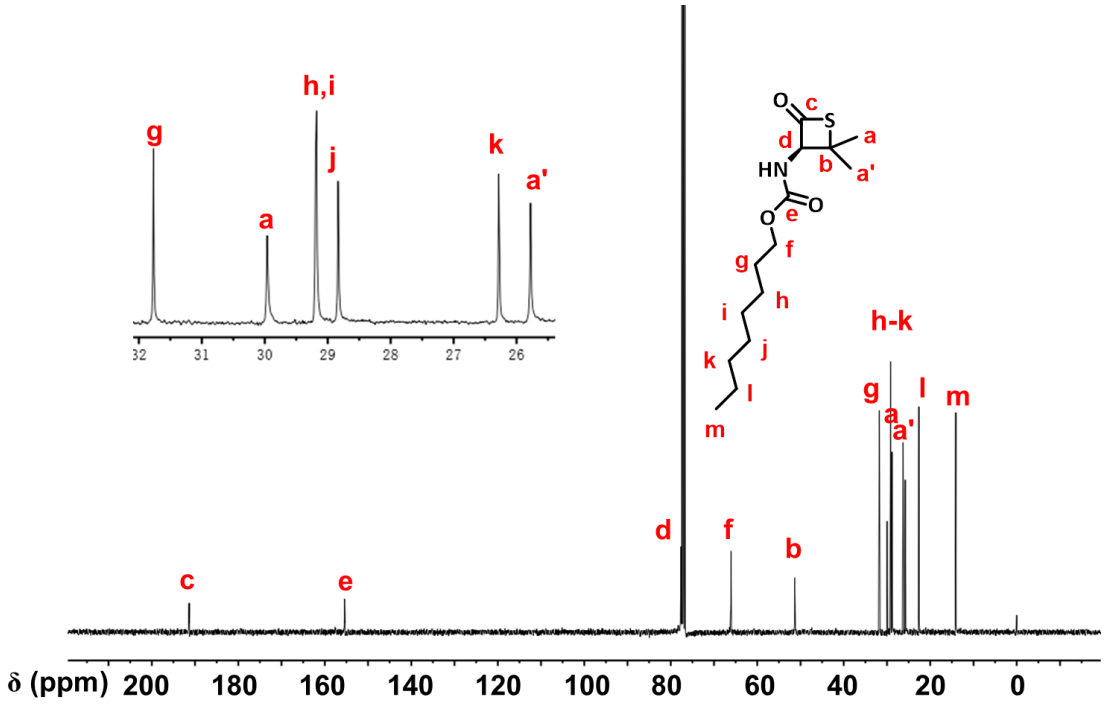


**Figure S8.** $^{13}$C NMR spectrum of N$^{C8}$-PenTL in $CDCl_3$.

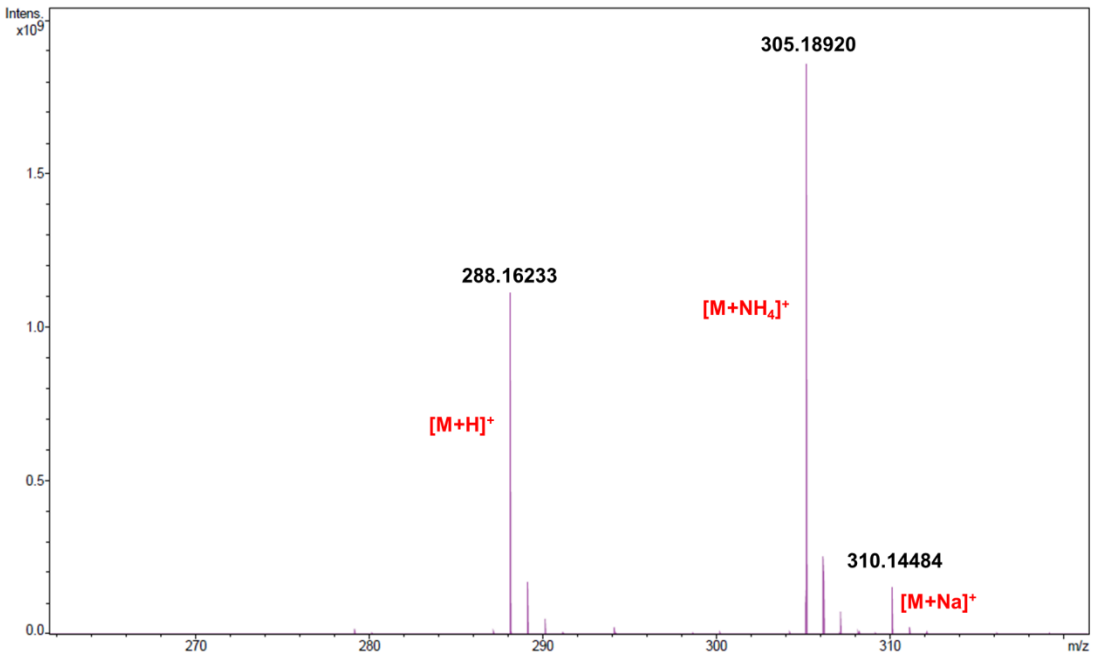


**Figure S9.** HR-MS spectrum of $N^{C8}$-PenTL.

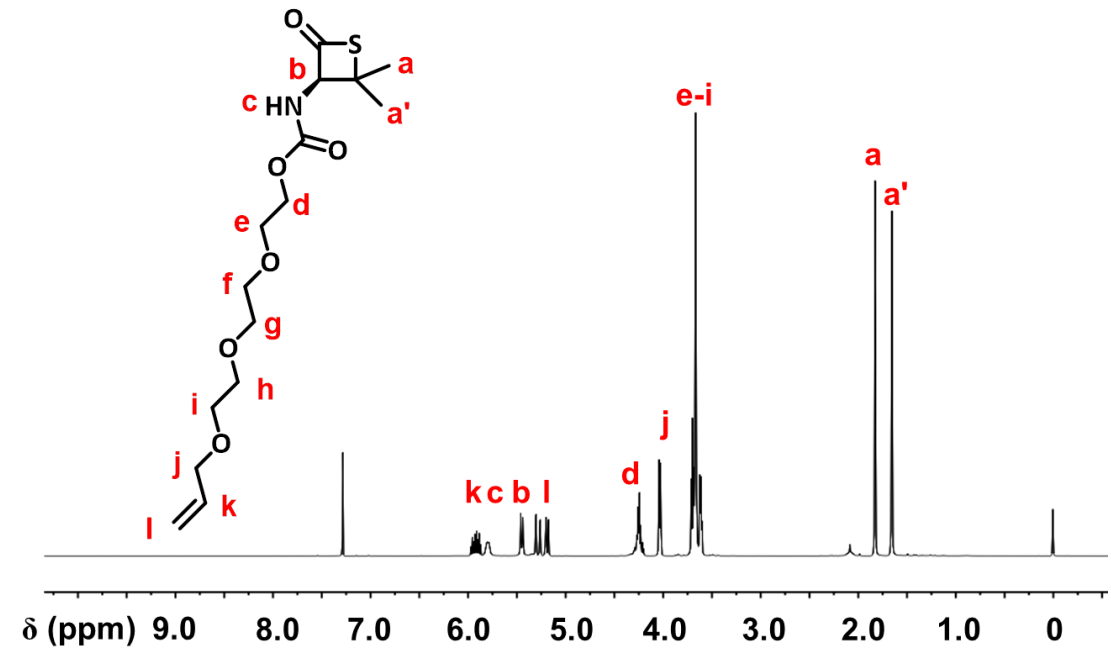


**Figure S10.** $^{1}$H NMR spectrum of N$^{ene}$-PenTL in $CDCl_3$.

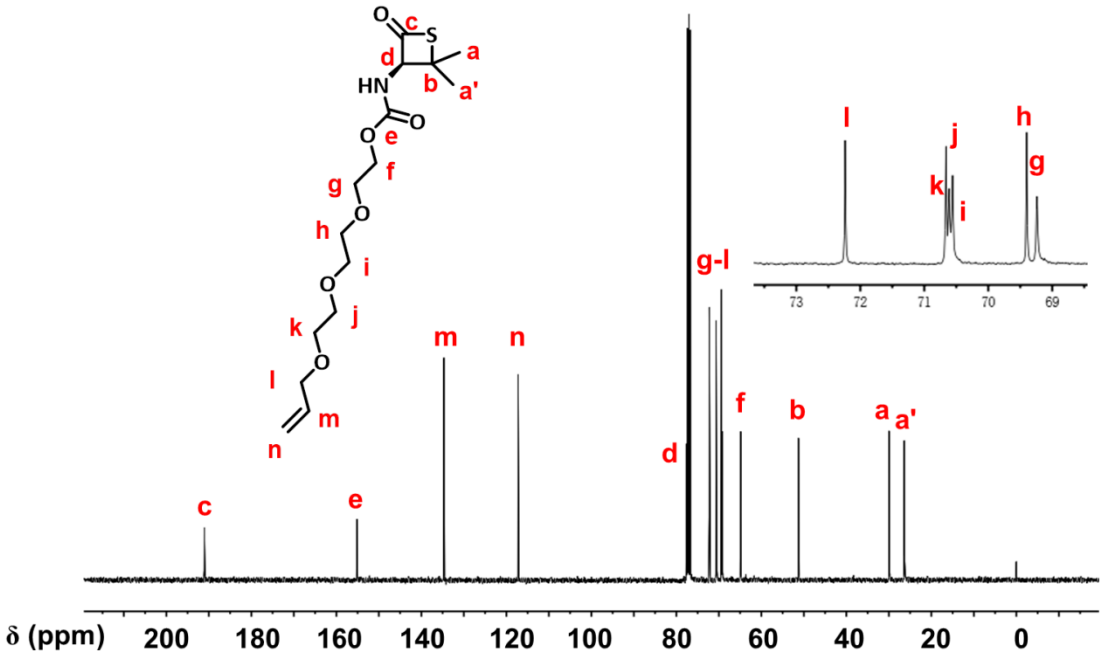


**Figure S11.** $^{13}$C NMR spectrum of N$^{ene}$-PenTL in $CDCl_3$.

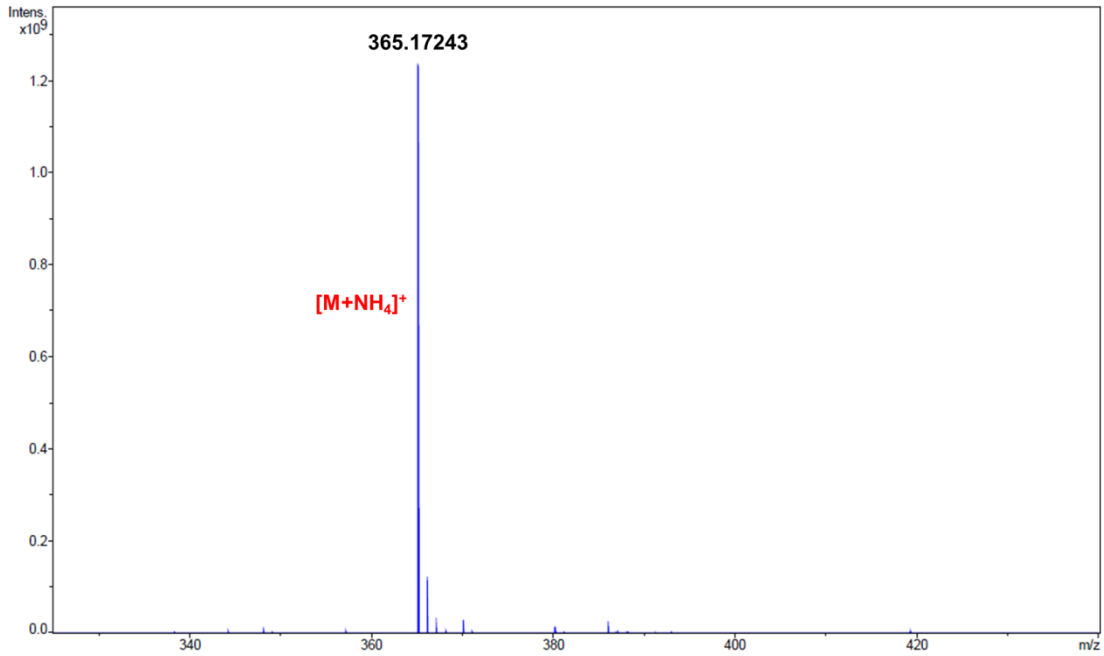


**Figure S12.** HR-MS spectrum of $N^{ene}$-PenTL.

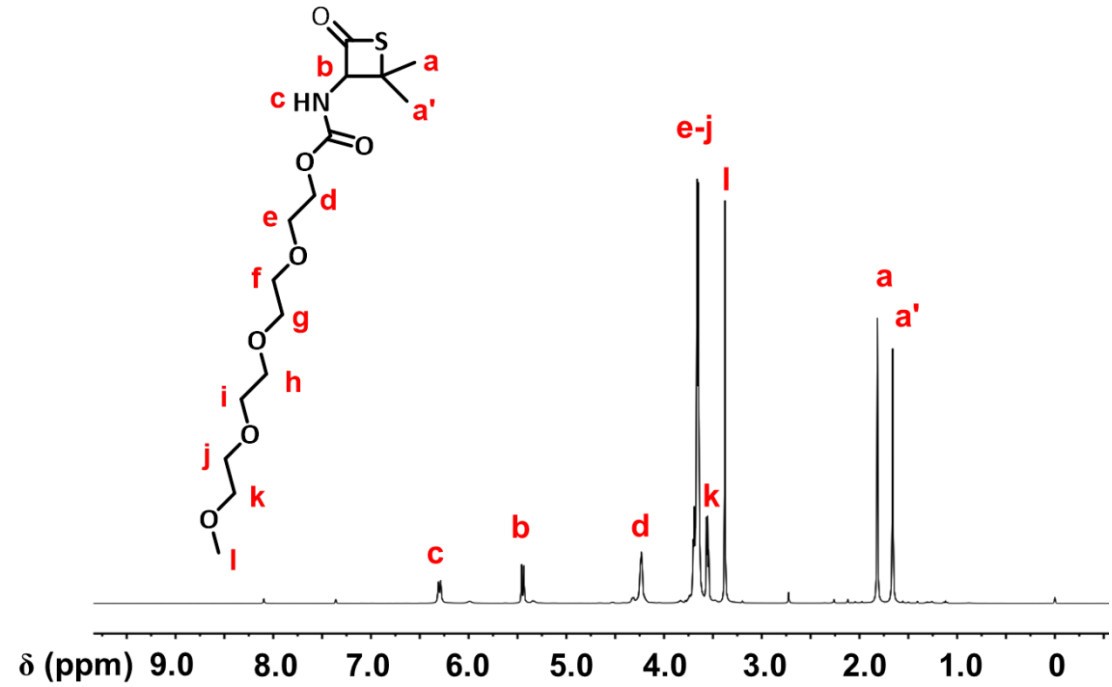


**Figure S13.** $^{1}$H NMR spectrum of $N^{EG4}$-PenTL in $CDCl_3$.

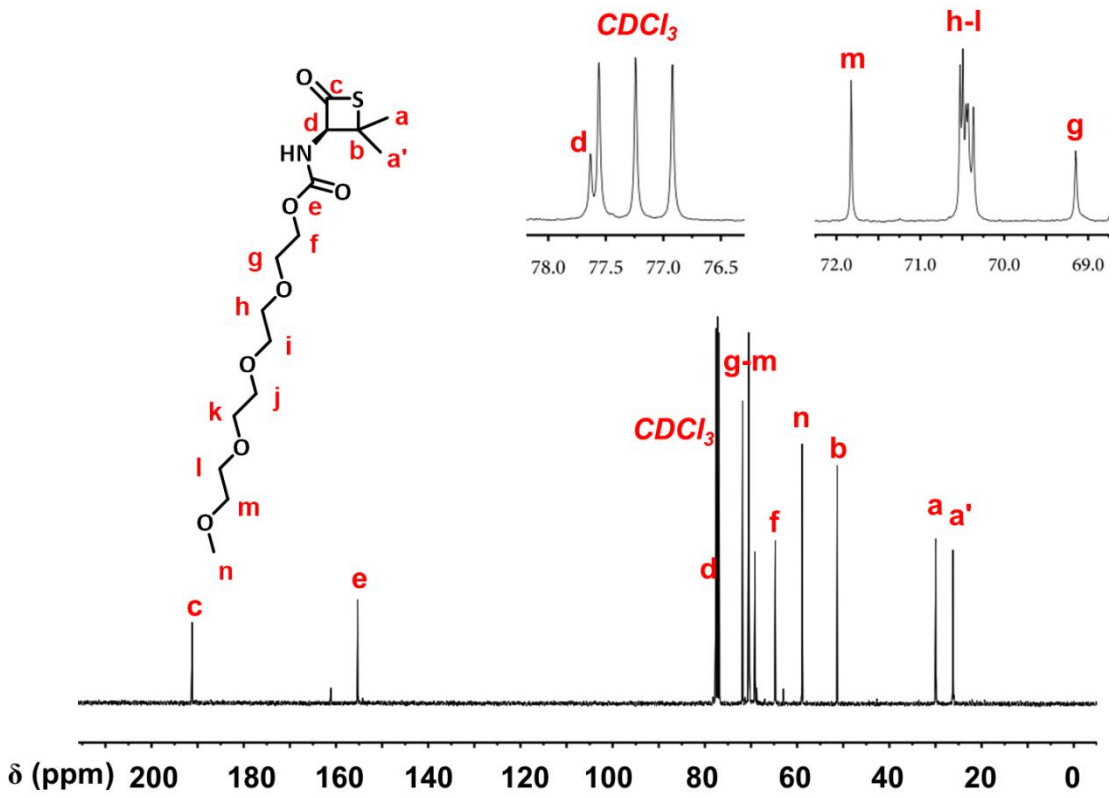


**Figure S14.** $^{13}$C NMR spectrum of $N^{EG4}$-PenTL in $CDCl_3$.

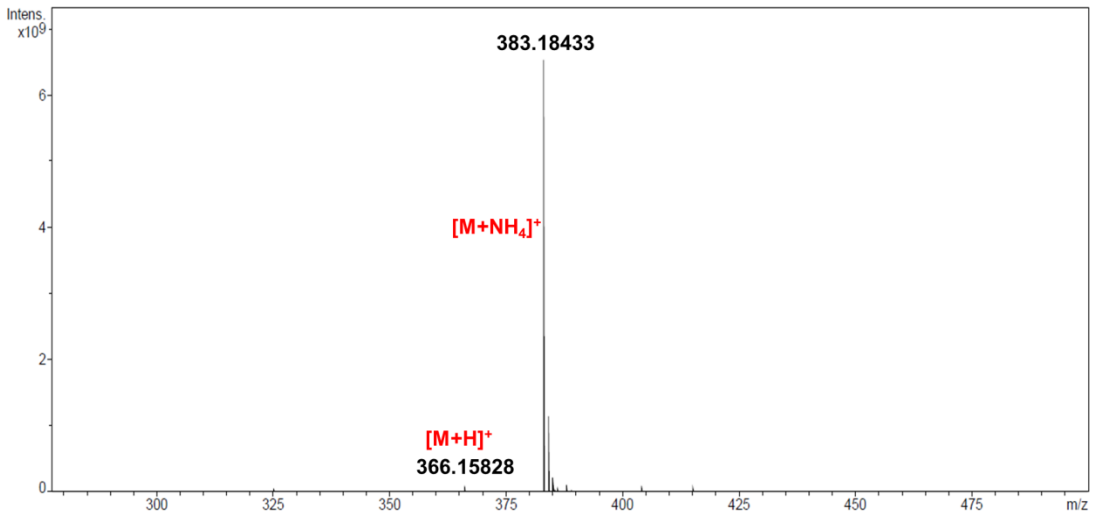


**Figure S15.** HR-MS spectrum of $N^{EG4}$-PenTL.

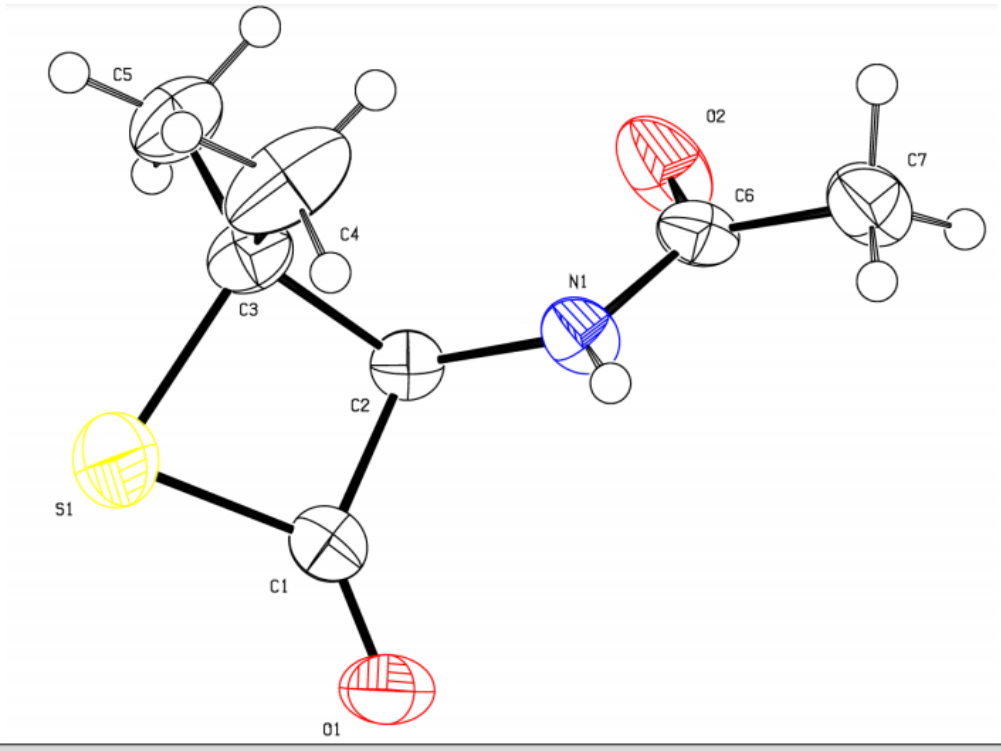


| | C1-C2 | C2-C3 | C3-S1 | S1-C1 | C1-O1 | C3-C4 | C3-C5 |
|---|---|---|---|---|---|---|---|
| Bond length (pm) | 152 | 157 | 186 | 177 | 119 | 151 | 151 |

| | C1-C2-C3 | C2-C3-S1 | C3-S1-C1 | S1-C1-C2 |
|---|---|---|---|---|
| Bond angle | 95.4 | 89.8 | 77.8 | 94.7 |

**Figure S16.** Thermal ellipsoid (50% probability) representations of $N^{Ac}$-PenTL.

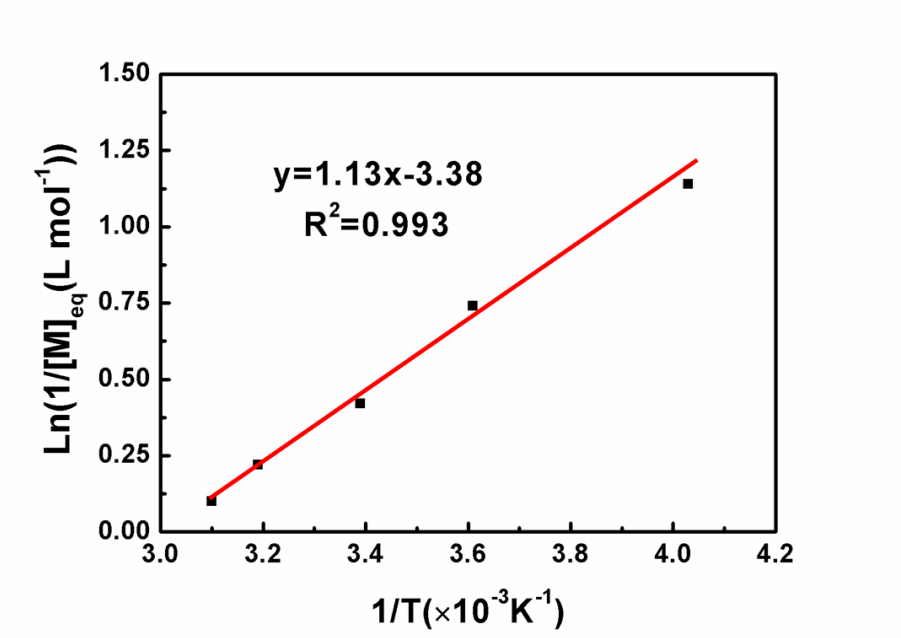


$$ln\left(\frac{1}{[M_{eq}]}\right) = \frac{-\Delta H_P^\circ}{RT} + \frac{\Delta S_P^\circ}{R}$$

**Figure S17**. Van't Hoff plot of ROP of $N^{ene}$-PenTL.

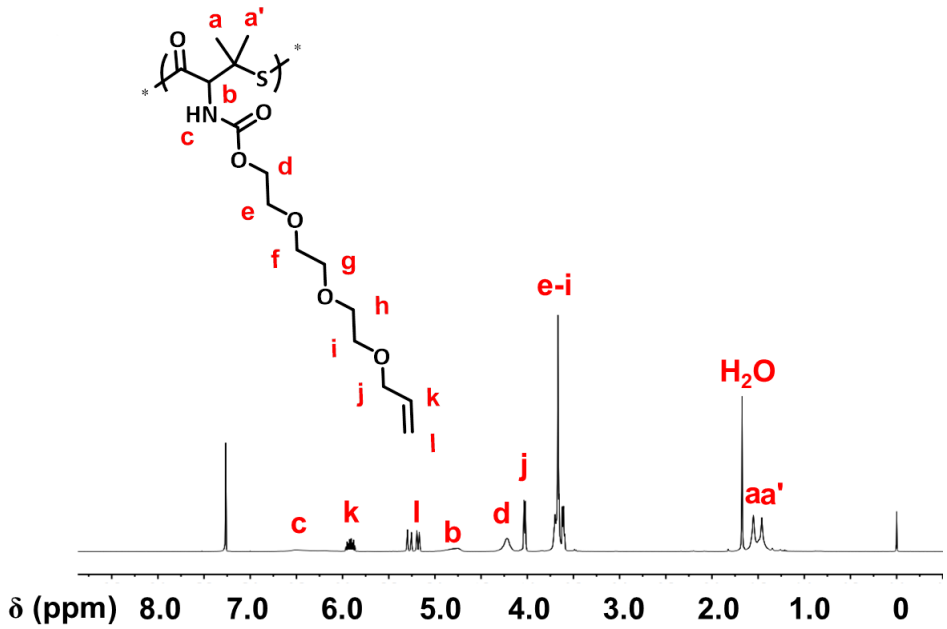


**Figure S18.** $^{1}$H NMR spectrum of PN$^{ene}$-PenTE in $CDCl_3$.

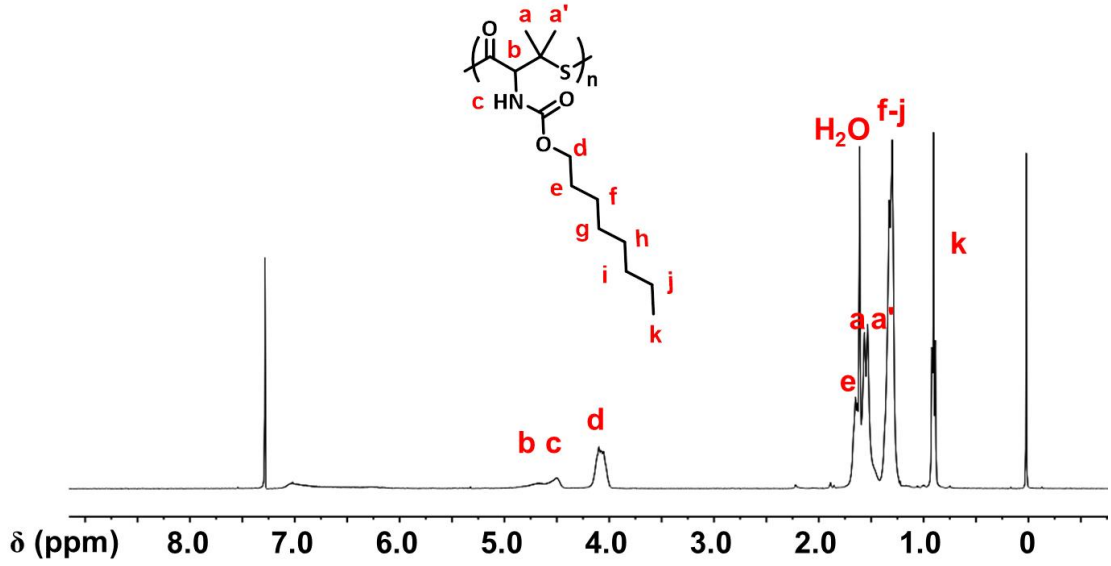


**Figure S19.** $^{1}$H NMR spectrum of PN$^{C8}$-PenTE in $CDCl_3$.

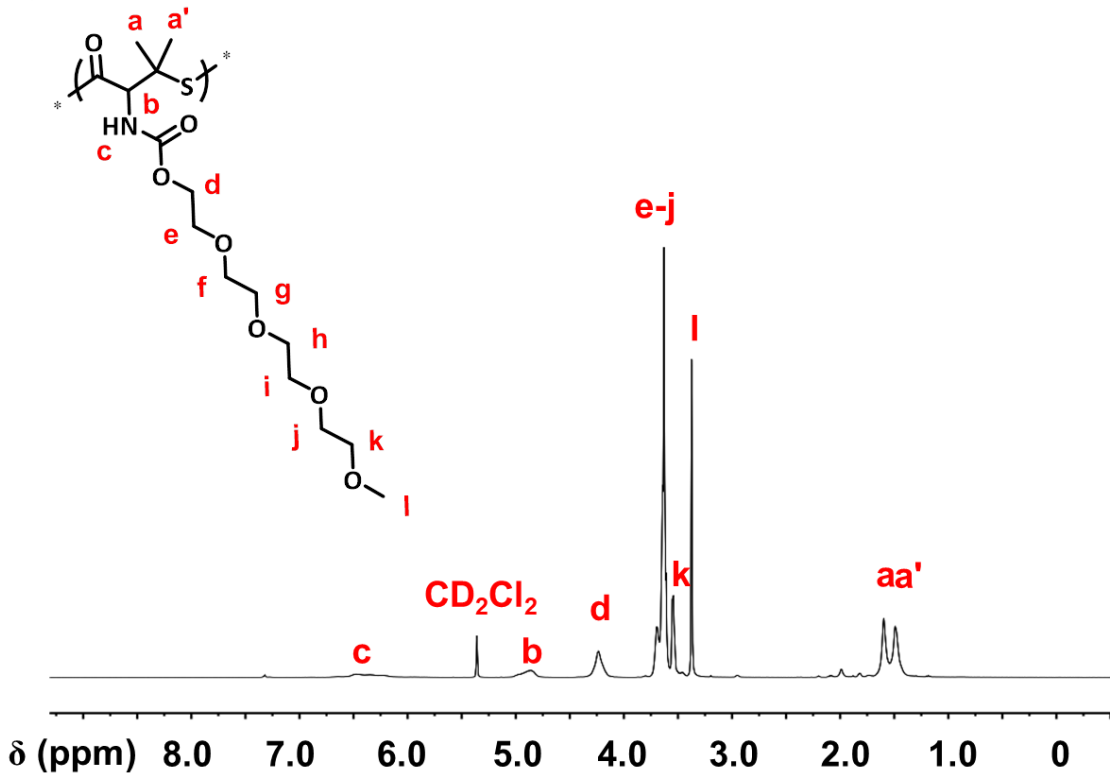


**Figure S20.** $^{1}$H NMR spectrum of PN$^{EG4}$-PenTE in $CD_2Cl_2$.

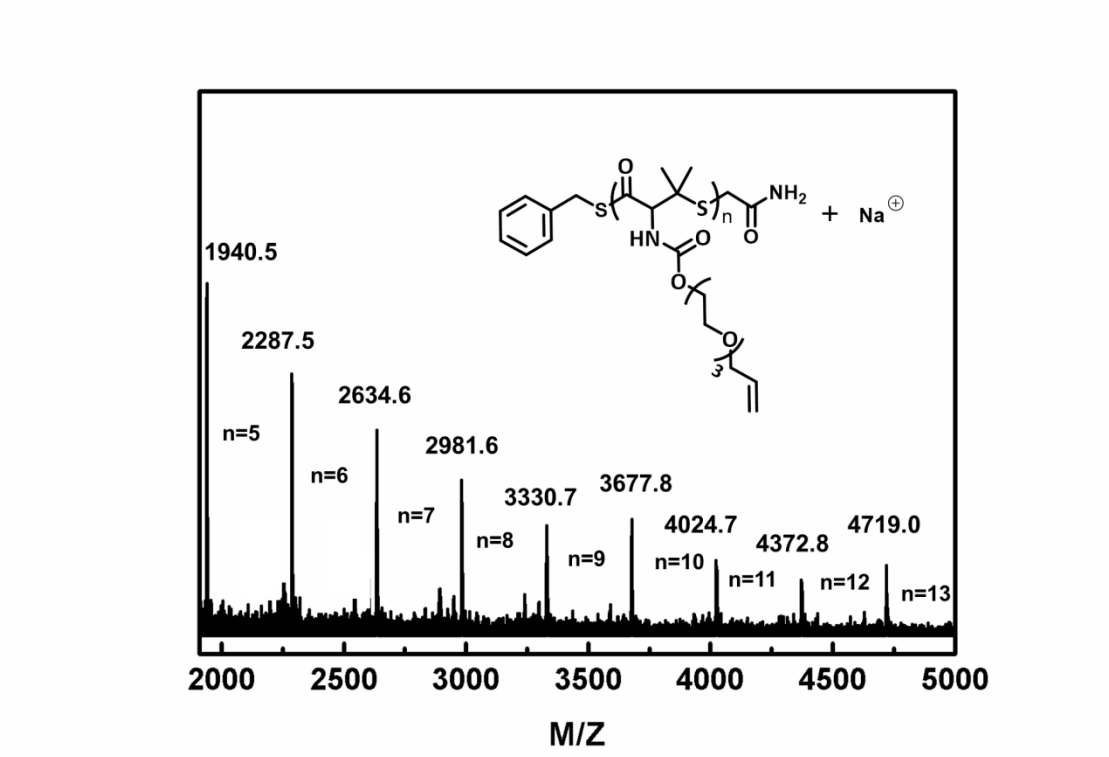


**Figure S21.** MALDI-TOF mass spectrum of $PN^{ene}$-$PenTE_{10}$ initiated by benzyl mercaptan and TEA, the ω-end was capped by iodoacetamide.

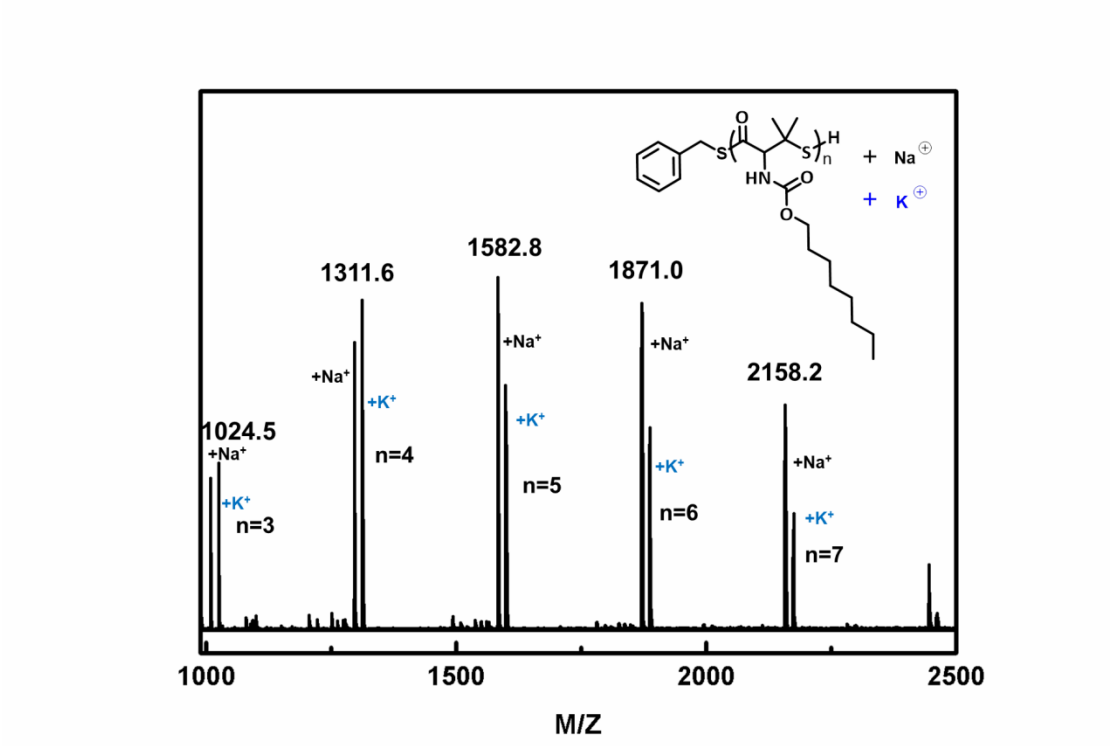


**Figure S22.** MALDI-TOF mass spectrum of $PN^{C8}$-$PenTE_{10}$ initiated by benzyl mercaptan and TEA.

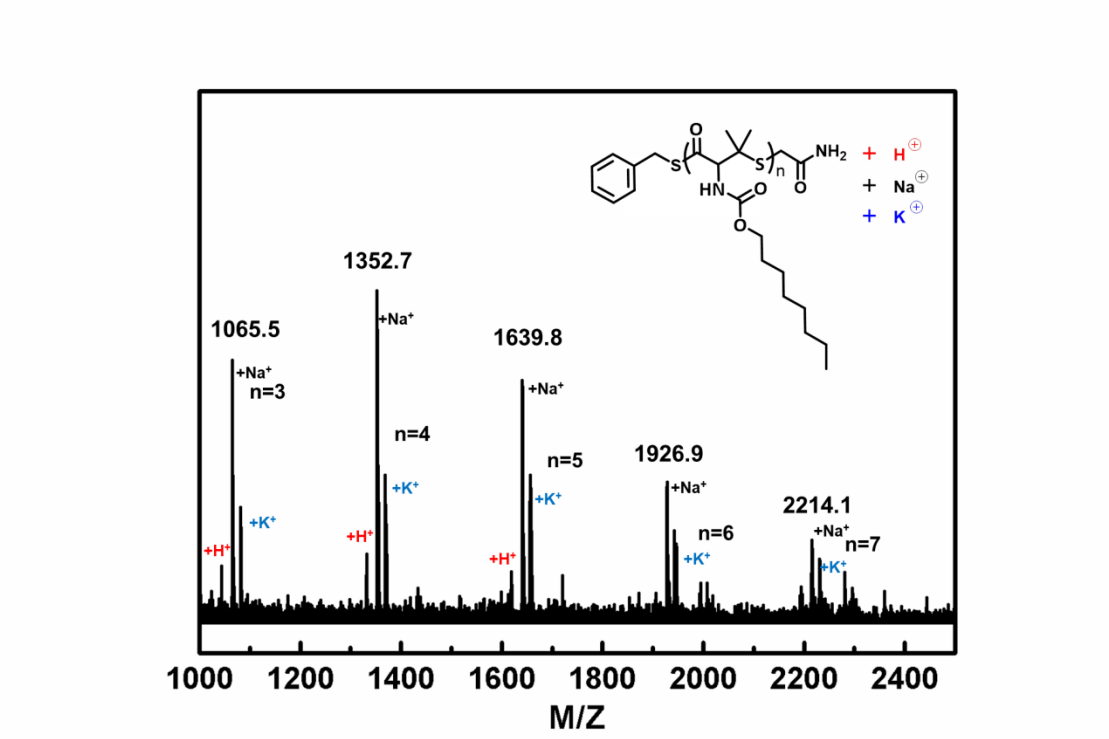


**Figure S23.** MALDI-TOF mass spectrum of $PN^{C8}$-$PenTE_{10}$ initiated by benzyl mercaptan and TEA; the ω-end was capped by iodoacetamide.

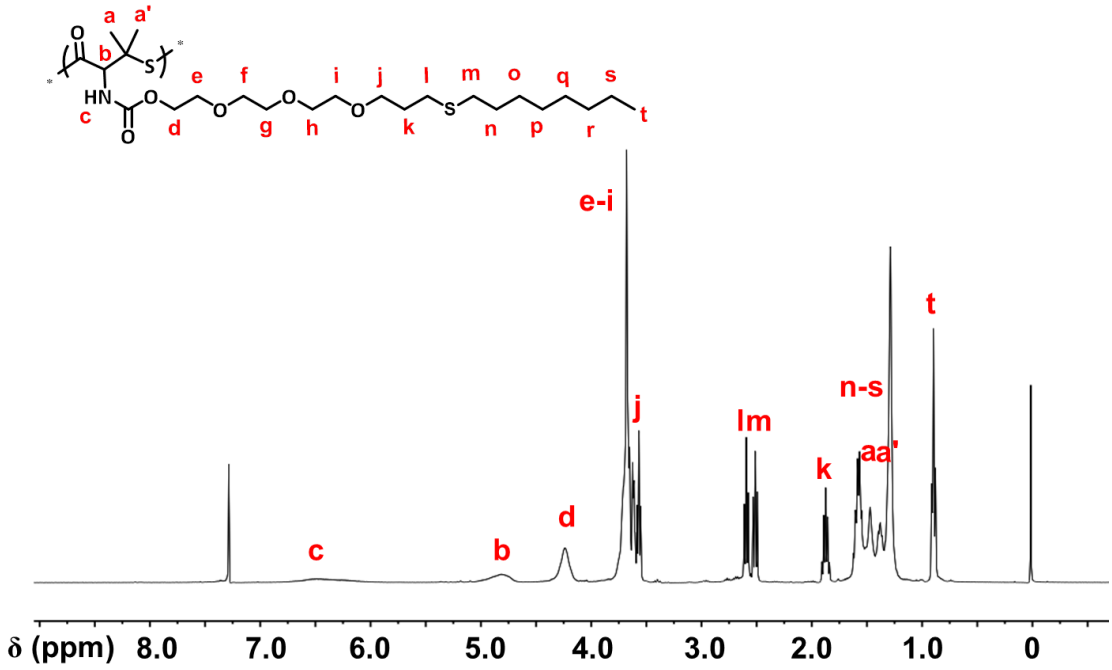


**Figure S24.** $^{1}$H NMR spectrum of PN$^{oct}$-PenTE in $CDCl_3$.

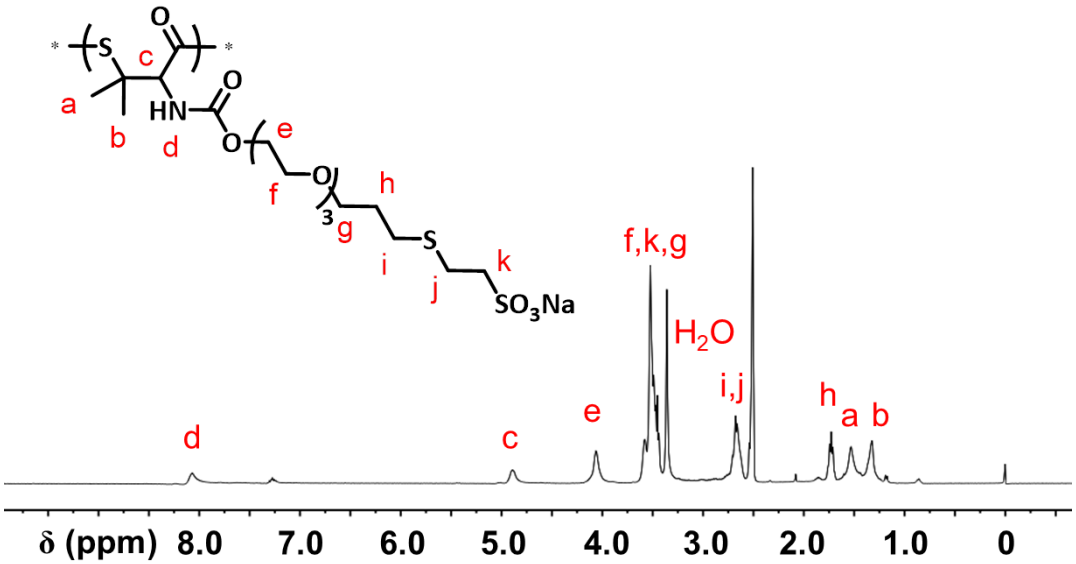


**Figure S25.** $^{1}$H NMR spectrum of PN$^{NaSO3}$-PenTE in $d_6$-DMSO.

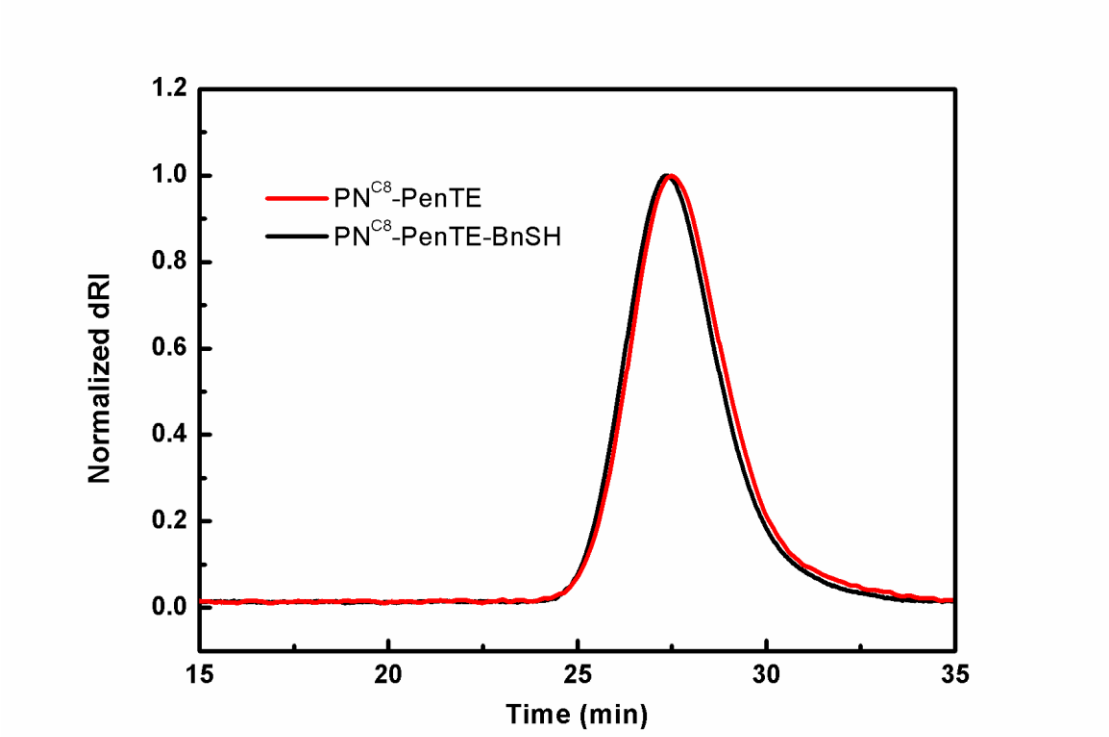


**Figure S26.** Overlay of the SEC traces of ω-end uncapped $PN^{C8}$-$PenTE_{150}$ before and after treating with 10 equiv benzyl mercaptan for 12 h at 65 °C.

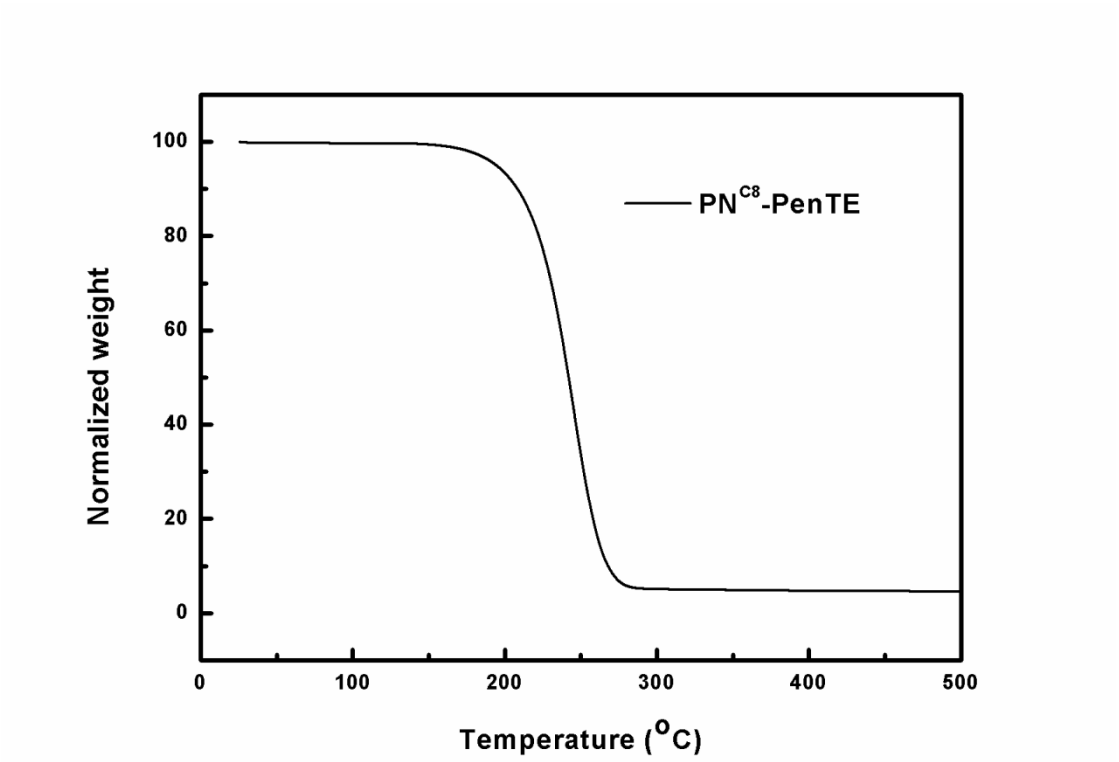


**Figure S27**. TGA traces of $PN^{C8}$-PenTE.

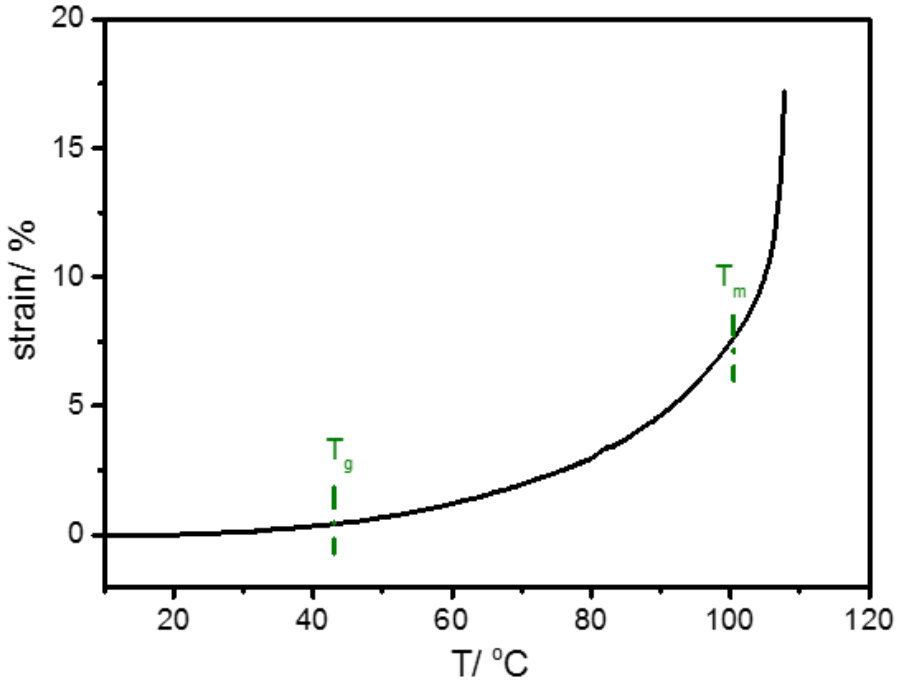


**Figure S28.** Dilatometry test of **PN$^{C8}$-PenTE** by DMA.

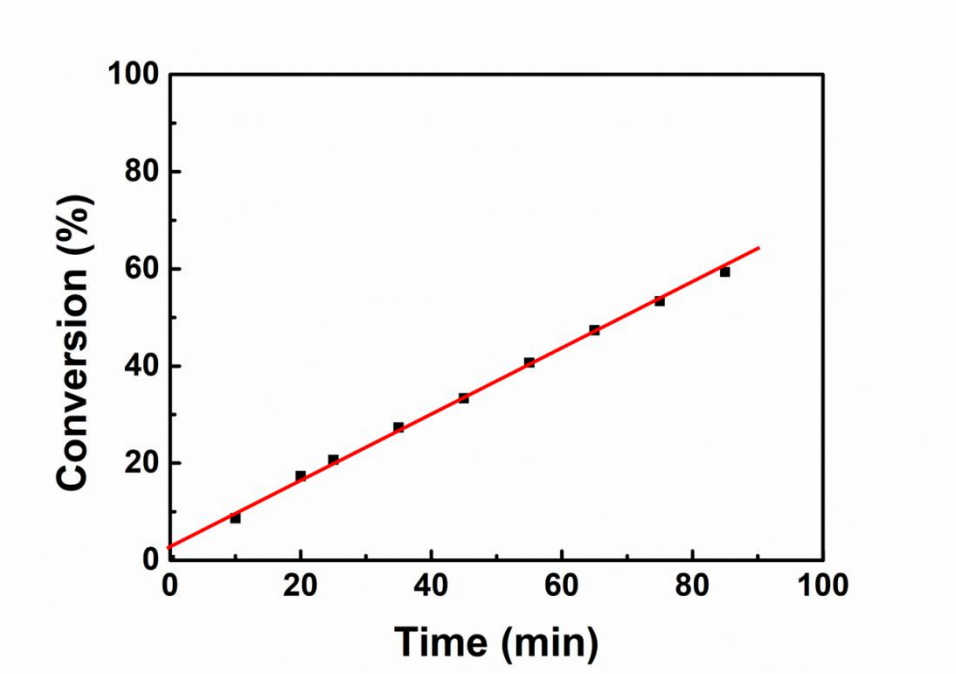


**Figure S29.** Kinetic plots of the depolymerization conversion of $PN^{C8}$-PenTE as a function of the reaction time.

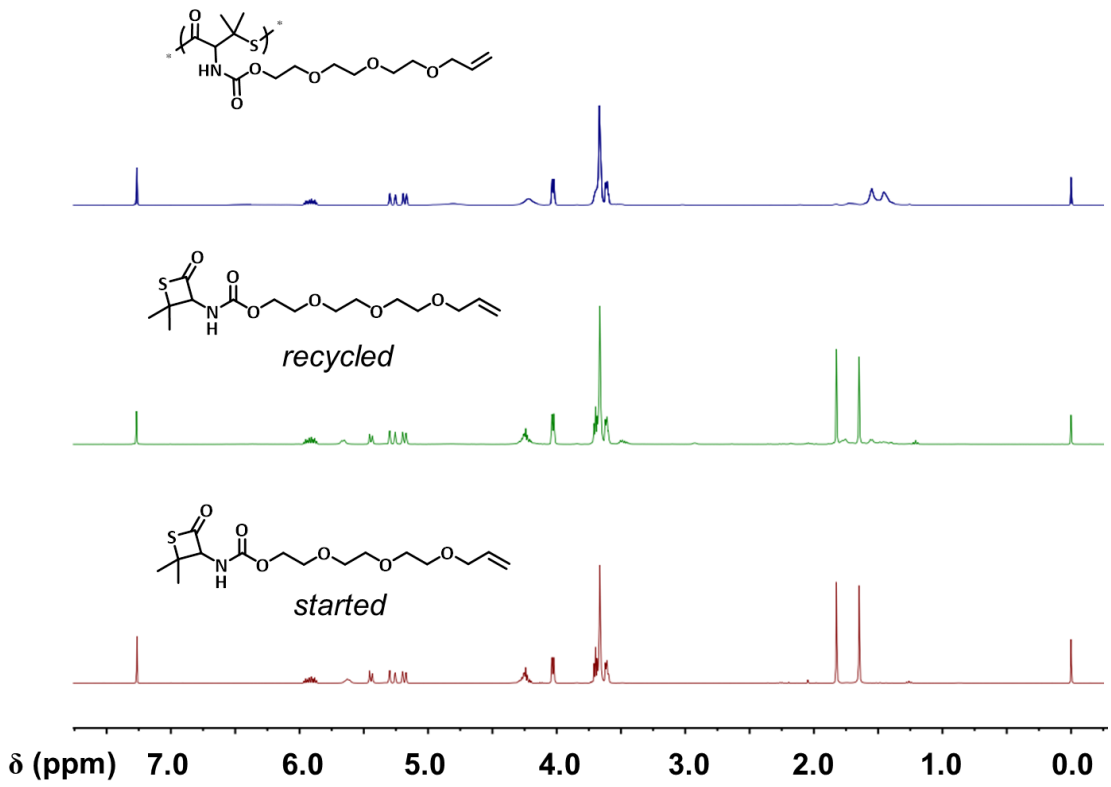


**Figure S30.** Overlay of the $^{1}$H NMR spectra of PN$^{ene}$-PenTE$_{50}$ (top), recycled N$^{ene}$-PenTL after treating the polymer with 0.1 equiv of DBU at 25 °C for 4 h (middle), and the started monomer N $^{ene}$-PenTL for comparison (bottom) in $CDCl_3$.

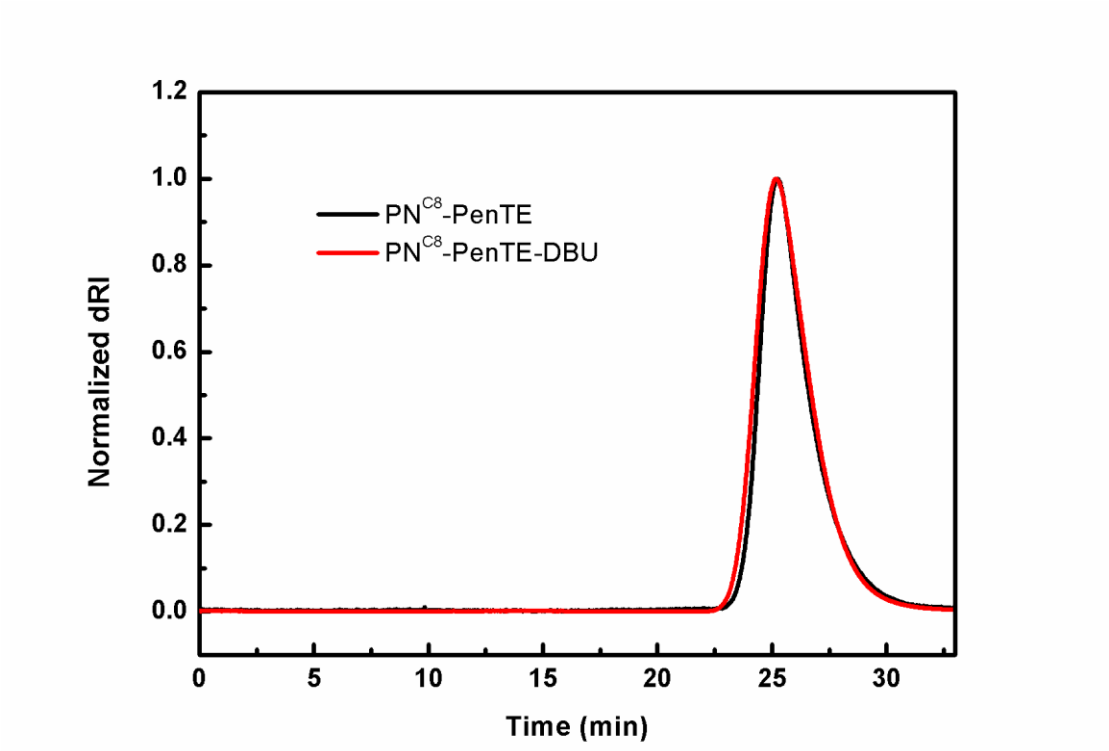


**Figure S31.** Overlay of the SEC curves of the ω-end capped $PN^{C8}$-$PenTE_{250}$ before and after treating with 0.1 equiv DBU for 12 h at 25 °C.

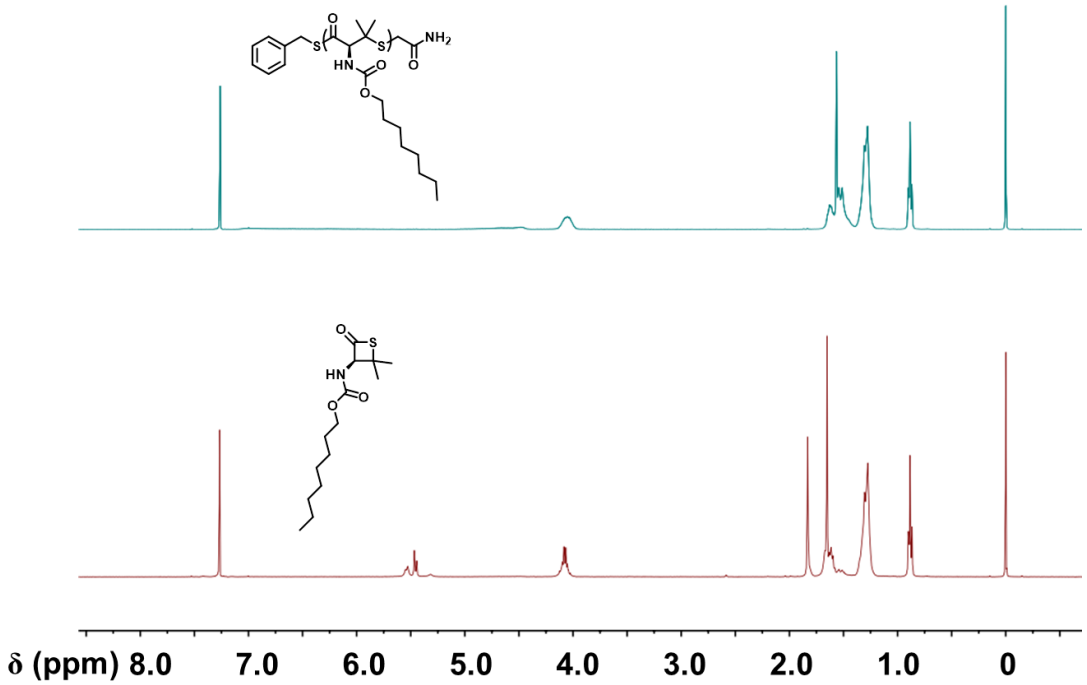


**Figure S32.** Overlay of $^{1}$H NMR spectra of the ω-end capped $PN^{C8}$-$PenTE_{50}$ (top) and recycled $N^{C8}$-PenTL after treating the polymer with 1 equiv of PhSNa at 25 °C for 2 h (bottom) in $CDCl_3$.

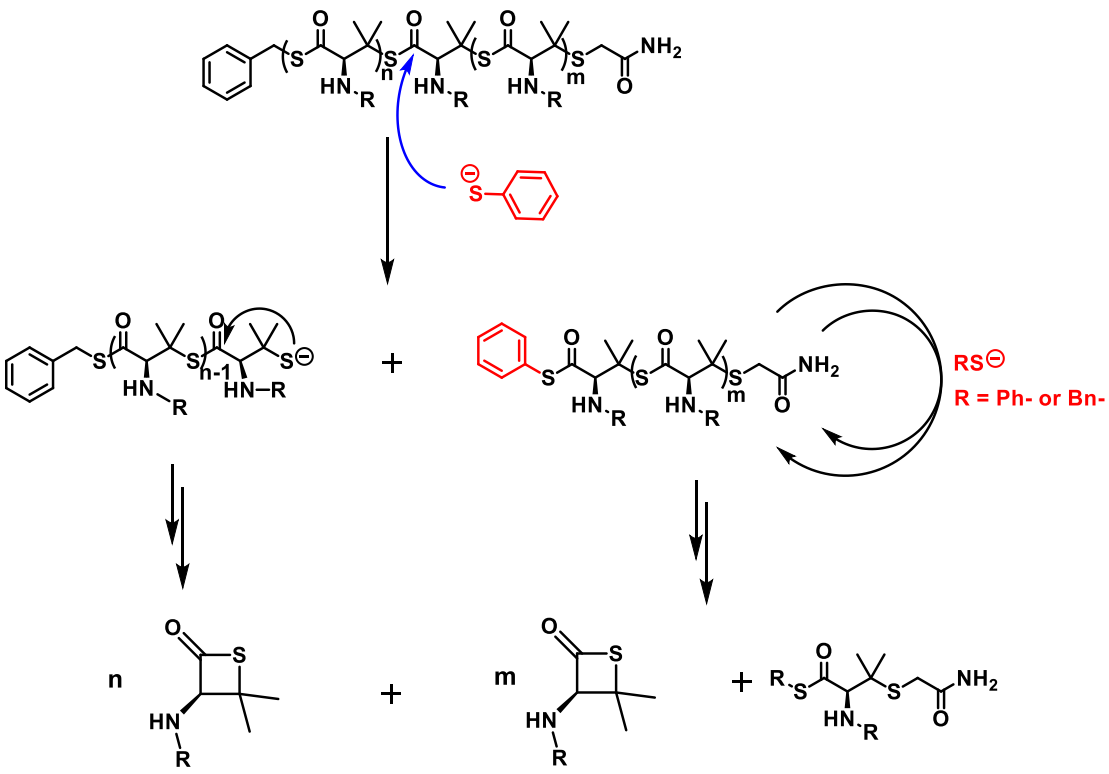


**Figure S33.** Proposed mechanism of the degradation of the ω-end capped PN$^{R}$-PenTE treated with PhSNa.

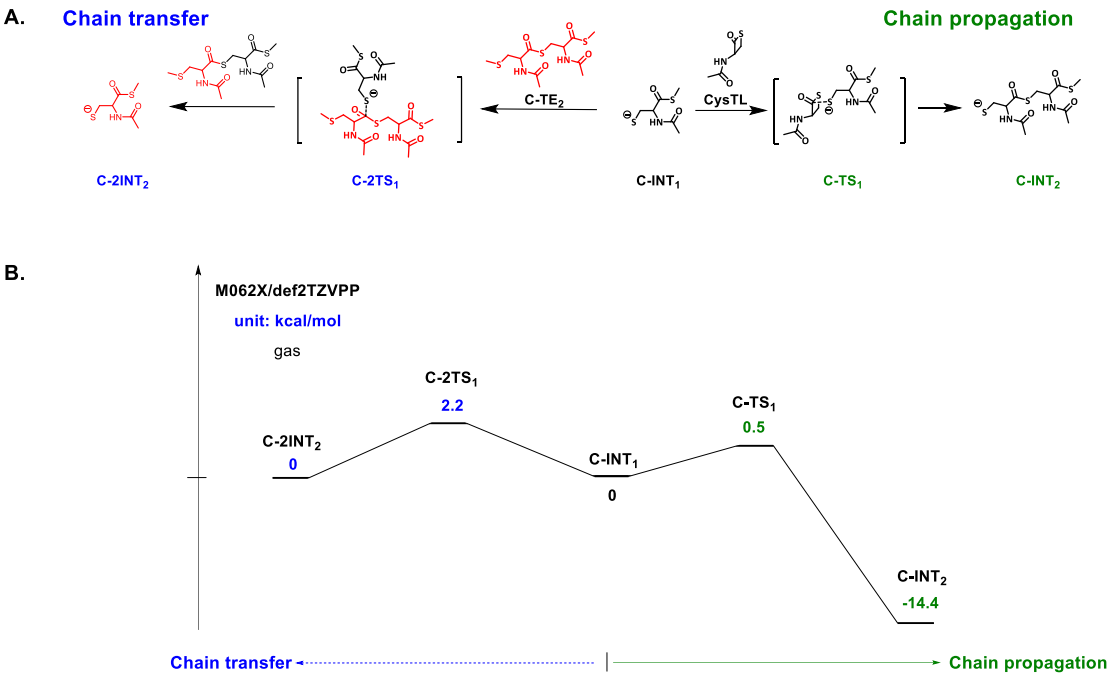


**Figure S34.** Mechanistic investigation of the ROP and chain transfer of $N^R$-CysTL by DFT calculation. (A) Plausible chain propagation and transfer intermediates (INT) and transition states (TS) in the ROP of $N^R$-CysTL in gas state. (B) Calculated free energy of each INT and TS.

## Supplemental Experimental Procedures

### Materials.

$_{D}$-Penicillamine ($_{D}$-Pen) was purchased from Innochem (Beijing, China). Benzyl mercaptan was purchased from J&K (Beijing, China). Di-*tert*-butyl dicarbonate, 1,8-diazabicyclo[5.4.0]undec-7-ene (DBU), 2,2-dimethoxy-2-phenylacetophenone (DMPA), triphosgene, and triethylene glycol were purchased from Aladdin Reagent Co. Ltd. (Shanghai, China). *t*BuP4 was purchased from Aldrich. (Shanghai, China). Anhydrous tetrahydrofuran (THF) and dichloromethane (DCM) were obtained by passing HPLC-grade solvents through columns packed with activated 4 Å molecular sieves.

### Characterizations.

NMR spectra were recorded on a 500 MHz AVANCE III or a 400 MHz Bruker ARX400 FT-NMR spectrometer. Size exclusion chromatography (SEC) experiments were performed on a system equipped with an isocratic pump (Model 1100, Agilent Technology, Santa Clara, CA), a DAWN HELEOS 9-angle laser light scattering detector (MALLS), Wyatt Technology, Santa Barbara, CA), and an Optilab rEX refractive index detector (Wyatt Technology, Santa Barbara, CA). The detection wavelength of MALLS was set at 658 nm. The temperature of both the refractive index and the MALLS detectors was 25 °C. Separations were performed using serially connected size exclusion columns (500, 103 ,104 , and 105 Å Phenogel columns, 5 μm, 7.8 × 300 mm, Phenomenex, Torrance, CA) at a flow rate of 1.0 mL/min and 50 °C using DMF containing 0.1 M LiBr as the mobile phase. The *d*n/*d*c values of P**N$^{C8}$-PenTE** and P**N$^{ene}$-PenTE**, calculated offline by using the internal calibration system (by the ASTRA V software version 5.1.7.3 provided by Wyatt Technology), were determined as 0.078 and 0.082 mL/g, respectively. Absolute molar masses ($M_n$) of all polymers were then determined based on their own *d*n/*d*c values. MALDI-TOF MS spectra were recorded on a Bruker Daltonics ultraflex TOF mass spectrometer in reflection mode with 2,5-dihydroxybenzoic acid (DHB) as the matrix (25 mg/mL in ACN/H2O = 70:30). 1.0 μL of polymer solution (1.0 mg/mL in THF) was mixed with 1.0 μL of matrix on the steel plate for MS analysis. Thermal gravimetric analysis (TGA) was performed on a TA Instrument Q600 analyzer. Samples were heated from ambient temperatures to 400 °C at a heating rate of 10 °C/min. Differential scanning calorimetry (DSC) analyses were performed on a METTLER TOLEDO Instrument DSC822 calorimeter with a heating rate of 10 °C/min. $T_g$ was obtained from the second heating scan after the thermal history was removed from the first heating scan. High-resolution mass spectra (HR-MS) were recorded on a Bruker Apex IV FTMS mass spectrometer. Crystallographic data of the compounds were collected on a Rigaku MM-07 Saturn 724 CCD diffractometer (Rigaku International Corp., Tokyo, Japan) using graphite-monochromated Mo Kα radiation.

### Synthesis of N$^{Ac}$-PenTL.

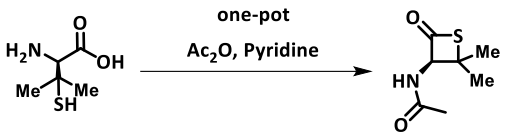


To an ice-cooled suspension of D-Pen (3.3 g, 22.1 mmol, 1.0 euqiv) in pyridine (12.5 mL) was added acetic anhydrous (5.8 mL, 61.5 mmol, 2.78 equiv) dropwise for 30 min. The solution was recovered to ambient temperature and stirred overnight. The resulting mixture was diluted with DCM (125 mL), washed with 1N HCl (60 mL), and followed by washing with saturated $NaHCO_3$ solution (60 mL). The organic layer was collected, dried over $Na_2SO_4$, and rotavapored under reduced pressure. The residue was recrystallized with THF/hexane (v/v 1/20) and obtained as a white crystal (1.7 g, yield 45%). $^1$H NMR (400 MHz, $CDCl_3$) δ7.46 – 6.17 (br, 1H), 5.69 (d, *J* = 8.1 Hz, 1H), 2.09 (s, 3H), 1.86 (s, 3H), 1.65 (s, 3H). $^{13}$C NMR (101 MHz, $CDCl_3$) δ 192.5, 169.6, 51.3, 30.2, 26.2, 22.6. ESI-MS: calculated m/z 173.1; found m/z 174.05831 $[M + H]^+$.

**Synthesis of $N^{Boc}$-PenTL.**

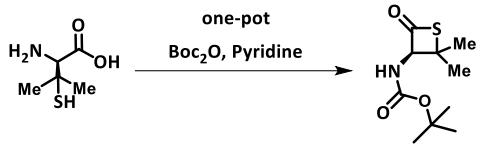


**$N^{Boc}$-PenTL** was prepared in a similar manner as **$N^{Ac}$-PenTL** excepting for replacing acetic anhydride with di-*tert*-butyl dicarbonate (2.78 equiv relative to D-Pen). **$N^{Boc}$-PenTL** was purified by recrystallization with THF/hexane (v/v 1/20) to afford a white crystal (1.2 g, 42% yield). $^1$H NMR (400 MHz, $CDCl_3$) δ 5.43 (d, *J* = 8.5 Hz, 1H), 5.18 (br, 1H), 1.85 (s, 3H), 1.63 (s, 3H), 1.47 (s, 9H). $^{13}$C NMR (101 MHz, $CDCl_3$) δ 191.7, 154.3, 80.9, 51.4, 30.1, 28.2, 26.3. ESI-MS: calculated m/z 231.1; found m/z 232.09995 $[M + H]^+$, 249.12648 $[M + NH_4]^+$, 254.08193 $[M + Na]^+$.

**Synthesis of $N^{ene}$-PenTL.**

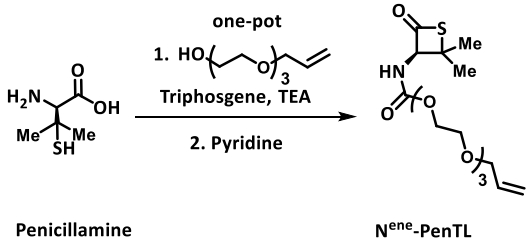


2-(2-(2-(allyloxy)ethoxy)ethoxy)ethanol was synthesized by following a procedure described previously.[1] To the solution of 2-(2-(2-(allyloxy)ethoxy)ethoxy)ethanol (5.7 g, 30.0 mmol) and triphosgene (3.0 g, 10.0 mmol) in THF was added TEA (3.1 g, 30.0 mmol) dropwise in an ice

bath. The mixture was stirred for 3 h to obtain the *suspension I*. In another vial, D-Pen (1.6 g, 10.0 mmol) was dispersed in pyridine (5.9 mL) under stirring rigorously to obtain the *suspension II*. The *suspension I* was dropped into the *suspension II* in an ice bath and continuously stirred overnight at ambient temperature. The mixture was added 60 mL DCM, and washed with 1N HCl (30 mL) followed by saturated $NaHCO_3$ solution (30 mL). The organic layer was collected, dried over $Na_2SO_4$, and rotavapored under reduced pressure. The residue was further purified by column chromatography (PE/EA=20/1) to afford pure $N^{ene}$-PenTL as a colorless oil (1.8 g, yield 49%). $^1$H NMR (400 MHz, $CDCl_3$) δ 5.92 (m, 1H), 5.80 (br, 1H), 5.45 (d, *J* = 8.8 Hz, 1H), 5.31 – 5.18 (dd, *J* = 10.4, 1.3 Hz, 2H), 4.24 (m, 2H), 4.03 (d, *J* = 5.7 Hz, 2H), 3.74 – 3.56 (m, 10H), 1.83 (s, 3H), 1.65 (s, 3H). $^{13}$C NMR (101 MHz, $CDCl_3$) δ 191.1, 155.2, 134.7, 117.2, 77.6, 72.2, 70.7, 70.6, 70.5, 69.4, 69.2, 64.9, 51.3, 29.9, 26.4. ESI-MS: calculated m/z 347.1; found m/z 365.17243 $[M + NH_4]^+$.

**Synthesis of $N^{C8}$-PenTL.**

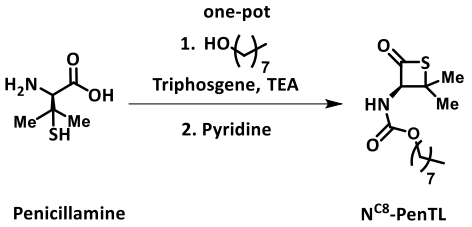


**$N^{C8}$-PenTL** was prepared in a similar manner as **$N^{ene}$-PenTL** excepting for replacing 2-(2-(2-(allyloxy)ethoxy)ethoxy)ethanol with *n*-octanol (3.0 equiv relative to D-Pen) as the starting material. **$N^{C8}$-PenTL** was purified by column chromatography (PE/EA=50/1) as colorless oil (7.1 g, yield 52%). $^1$H NMR (400 MHz, $CDCl_3$) δ 5.67 – 5.47 (m, 2H), 4.09 (m, 2H), 1.85 (s, 3H), 1.70 – 1.40 (m, 5H), 1.42 – 1.22 (m, 10H), 0.90 (t, *J* = 6.8 Hz, 3H). $^{13}$C NMR (101 MHz, $CDCl_3$) δ 191.3, 155.4, 77.6, 66.1, 51.4, 31.8, 29.9, 29.2, 28.8, 26.3, 25.8, 22.7, 14.1. ESI-MS: calculated m/z 287.2; found m/z 288.16233 $[M + H]^+$, 305.18920 $[M + NH_4]^+$, 310.14484 $[M + Na]^+$.

**Synthesis of $N^{EG4}$-PenTL.**

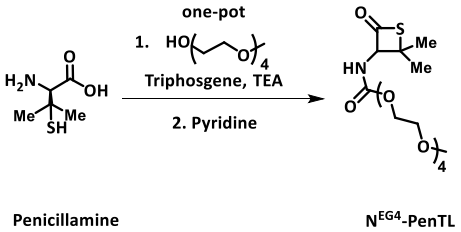


**$N^{EG4}$-PenTL** was prepared in a similar manner as **$N^{ene}$-PenTL** excepting for replacing 2-(2-(2-(allyloxy)ethoxy)ethoxy)ethanol with methyl tetraglycol (3.0 equiv relative to D-Pen) as the starting material. **$N^{EG4}$-PenTL** was purified by column chromatography (PE/EA=20/1) as colorless oil (3.1 g, yield 46%). $^1$H NMR (400 MHz, $CDCl_3$) δ 6.30 (d, *J* = 8.8 Hz, 1H), 5.45 (d, *J* = 8.9 Hz, 1H), 4.28 – 4.16 (m, 2H), 3.79 – 3.59 (m, 12H), 3.58 – 3.49 (m, 2H), 3.38 (s, 3H), 1.82 (s, 3H), 1.66 (s, 3H). $^{13}$C NMR (101 MHz, $CDCl_3$) δ 191.2, 155.3, 77.6, 70.5(3), 70.4(9),

70.4(6), 70.4(3), 70.3(7), 64.7, 58.9, 51.3, 29.9, 26.2. ESI-MS: calculated m/z 365.2; found m/z 366.15828 $[M + H]^+$, 383.18433 $[M + NH_4]^+$.

**General procedure for the ring-opening polymerization of $N^R$-PenTL.**

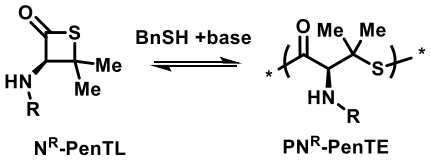


In a glovebox, benzyl mercaptan (2.0 M, 29.5 μL, 1.0 equiv) and DBU (2.0 M, 3.0 μL, 0.10 equiv) in THF was added to $N^{C8}$-PenTL (1740 mg, 0.35 mmol, 100 equiv). The polymerization was kept at ambient temperature for 24 h. Upon reaching equilibrium, iodoacetamide (1.0 M, 300 μL, 5.0 equiv) in THF or trifluoroacetic acid (1.0 equiv) was added to quench the polymerization. The mixture was diluted with DCM (10 mL), precipitated in isopropanol (450 mL), and collected with centrifugation. The crude product was further purified by repeating the solution-precipitation-centrifugation cycle twice to obtain a white solid before drying under vacuum (920 mg, yield 53%). $^1$H NMR (400 MHz, $CDCl_3$) δ 7.06 (br, 1H), 4.50 (m, 1H), 4.33-3.79 (m, 2H), 1.75-1.44 (m, 6H), 1.41-1.21 (m, 8H), 0.91 (t, *J* = 6.7 Hz, 3H).

**$PN^{ene}$-PenTE** was synthesized in a similar manner excepting for using diethyl ether rather than isopropanol for polymer precipitation (yield 43%). $^1$H NMR (400 MHz, $CDCl_3$) δ 6.75 (br, 1H), 6.00-5.84 (m, 1H), 5.18 (dd, *J* = 10.4, 1.3 Hz, 1H), 5.13 (dt, *J* = 100.0, 50.0 Hz, 1H), 4.81 (m, 1H), 4.22 (m, 2H), 4.10-3.95 (m, 2H), 3.82-3.50 (m, 10H), 1.70-1.46 (m, 3H), 1.45-1.35 (m, 3H).

**$PN^{EG4}$-PenTE** was also synthesized in a similar manner excepting for using diethyl ether rather than isopropanol for polymer precipitation (yield 41%). $^1$H NMR (400 MHz, $CD_2Cl_2$) δ 6.41 (br, 1H), 4.86 (m, 1H), 4.23 (m, 2H), 3.76 – 3.58 (m, 12H), 3.57 – 3.49 (m, 2H), 3.37 (m, 3H), 1.60 (m, 3H), 1.49 (m, 3H).

**Post-polymerization modification of $PN^{ene}$-PenTE via the thiol-ene reaction.**

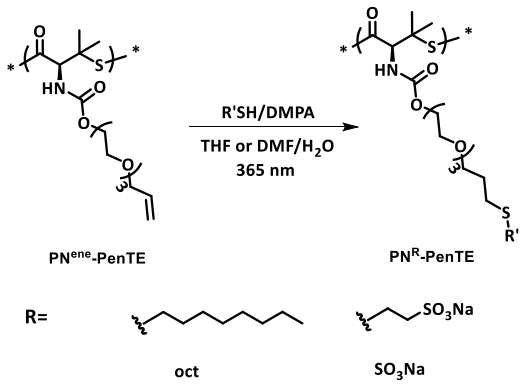

To a solution of **PN$^{ene}$-PenTE$_{50}$** (20.0 mg, 0.058 mmol 'ene', 1.0 equiv) in THF (1 mL) was added *n*-octyl mercaptan (34 mg, 0.29 mmol, 5.0 equiv) and DMPA (1 M, 2.9 μL, 0.05 equiv.) in THF under stirring. The resulting mixture was exposed in UV irradiation (365 nm, 1 W/cm$^2$) for 2 h before precipitation in hexane. The precipitate was collected by centrifugation and redissolved in THF. The crude product was further purified by repeating the dissolving-precipitation-centrifugation cycle twice to afford pure PN$^{oct}$-PenTE as a colorless oil (21 mg, 80% yield). $^1$H NMR (400 MHz, $CDCl_3$) δ 6.48 (br, 1H), 4.82 (br, 1H), 4.39 – 4.06 (m, 2H), 3.80 – 3.59 (m, 10H), 3.57 (t, *J* = 6.3 Hz, 2H), 2.59 (t, *J* = 7.3 Hz, 2H), 2.51 (t, *J* = 7.3 Hz, 1H), 1.97 – 1.78 (m, 2H), 1.69 – 1.13 (m, 18H), 0.90 (t, *J* = 6.7 Hz, 3H).

Thiol-ene modification of **PN$^{ene}$-PenTE** with sodium 2-mercaptoethanesulfonate was carried out in a similar manner using DMF as the solvent. For purification, the reaction mixture was dialyzed against DI water and lyophilized to afford pure **PN$^{SO3Na}$-PenTE** as a white solid (22 mg, 75% yield). $^1$H NMR (400 MHz, DMSO) δ 8.09 (m, 1H), 4.90 (m, 1H), 4.06 (m, 2H), 3.78 – 3.41 (m, 14H), 2.91 – 2.36 (m, 4H), 1.81 – 1.65 (m, 2H), 1.53 (m, 3H), 1.32 (m, 3H).

**Thermodynamic study of the ROP**

**N$^{ene}$-PenTL** (20 mg, 0.057 mmol, 10 equiv) in THF (24 μL) was mixed with benzyl mercaptan (2.0 M, 2.9 μL, 1 equiv) and DBU (0.20 M, 2.9 μL, 1 equiv) in THF. The reaction was evenly divided into five portions (10 μL) and incubated at -25, 0, 4, 25, and 50 °C for 3h, respectively. The resulting mixture was quenched by iodoacetamide (1.0 M, 29 μL, 5 equiv) in THF and the equilibrium monomer concentration ($[M]_{eq}$) at each temperature was measured by $^1$H NMR. The thermodynamic parameters such as $\Delta H_P°$ and $\Delta S_P°$ were calculated by plotting the logarithm of the reciprocal of the equilibrium monomer concentration ($\ln(1/[M]_{eq})$) with the reciprocal of temperature ($1/T$) according to the Van't Hoff equation.

**Kinetic study of depolymerization of PN$^{C8}$-PenTE catalyzed by DBU.**

To the solution of **PN$^{C8}$-PenTE$_{150}$** (25 mg, 1.0 euqiv) in $CDCl_3$ (25 mL) was added DBU (0.01 M, 2.8 μL, 0.05 equiv relative to the polymer chain number) in $CDCl_3$ at 60 °C. To monitor the depolymerization kinetics, an aliquot (5 mL) of the mixture was taken out at different time intervals and quenched with iodoacetamide (0.01 M, 28 μL, 5 equiv) in $CDCl_3$. The mixtures were concentrated to ~500 μL under vacuum before $^1$H NMR analysis. Next, the $CDCl_3$ solution of each portion was evaporated under vacuum and redissolved in DMF (1.0 mL) containing 0.1 M LiBr for SEC analysis.

**Preparation of films.**

A sample of **PN$^{C8}$-PenTE** (120 mg) was put into a customized mold with a rectangular hole of 25 mm × 20 mm and 0.2 mm in thick. Fixed by two pieces of aluminum plates, the mold was placed in a hot plate at 140 °C and 0.6 MPa pressure force. After 15 min, the sample was

allowed cooling down to room temperature and the pressure was removed. A transparent film with a scale of 25 mm × 20 mm × 0.20 mm was obtained.

**Dilatometry experiment.**

Dilatometry experiment was performed on a TA-Q800 DMA apparatus under a constant of 50 kPa. The size of the **PN$^{C8}$-PenTE** film was 4.50 mm × 4.30 mm × 0.19 mm. The strain was measured from 10 to 110 $^{o}$C at a heating rate of 3 $^{o}$C/min. The increases of the curve slope represented the glass transition ($T_g$) and melting transition ($T_m$), respectively.

**Tensile test of PN$^{C8}$-PenTE.**

A rectangular spline with a scale of 10 mm × 4 mm × 0.2 mm was obtained by cutting the film at 80 $^{o}$C. The tensile test was performed on a TA-Q800 DMA apparatus with a force ramping rate of 0.5 N/min.

**Molecular Dynamics simulation method.**

We used the Amber 14 Molecular Dynamics Package to perform the all-atom simulation of PN$^{Me}$-PenTE$_{20}$. The PN$^{Me}$-PenTE$_{20}$ molecule was modeled with GAFF.[2] And the charges on all atoms in PN$^{Me}$-PenTE$_{20}$ molecule were obtained using the RESP-fit[3, 4] method based on HF/6-31G* calculations. A chain of PN$^{Me}$-PenTE$_{20}$ molecules were then generated using teLeap program included in AMBER Tools 15. The whole system was placed in a box with periodic boundary conditions and solvated by chloroform.[5] The initial structure of PN$^{Me}$-PenTE$_{20}$ molecule was first subjected to 5000 steps of minimization, and then the temperature of the system was established by velocity rearrangement from a Maxwell-Boltzmann distribution at 300 K. After these preparing steps the system was maintained at 300 K using the Langevin dynamics with a coupling constant of 2 ps$^{-1}$. In MD simulations, the SHAKE[6] algorithm with a relative geometric tolerance of $10^{-5}$ was used to constrain all chemical bonds. Thus, all dynamics utilized a 2 fs time step. Long-range electrostatics was treated by the particle-mesh Ewald (PME)[7] method with default settings and a 10 Å direct space nonbonded cutoff was used in all simulations.

**Computational details.**

All calculations were carried out with density functional theory (DFT) in GAUSSIAN 09 software package.[8] Geometry optimizations and frequency calculations of intermediates (INT) and transition states (TS) were performed with 6-31+G(d) basis set and B3LYP functional.[9] To further obtain Gibbs free energies (kcal/mol) with a high degree of accuracy, single-point calculations were then done using the M06-2X functional[10] with the def2TZVPP basis set.

**Supplemental References:**


1. Yuan, J., Zhang, Y., Sun, Y., Cai, Z., Yang, L., and Lu, H. (2018). *Biomacromolecules*, *19*, 2089-2097.
2. Wang, J. M., Wolf, R. M., Caldwell, J. W., Kollman, P. A., and Case, D. A. (2004). *J. Comput. Chem. 25*, 1157-1174.
3. Singh, U. C., and Kollman, P. A. (1984). *J. Comput. Chem. 5*, 129-145.
4. Besler, B. H., Merz, K. M., and Kollman, P. A. (1990). *J. Comput. Chem. 11*, 431-439.
5. Cieplak, P., Caldwell, J., and Kollman, P. (2001). *J. Comput. Chem. 22*, 1048-1057.
6. Ryckaert, J. P., Ciccotti, G., and Berendsen, H. J. C. (1977). *J. Comput. Phys. 23*, 327-341.
7. Darden, T., York, D., and Pedersen, L. (1993). *J. Chem. Phys. 98*, 10089-10092.
8. Frisch, M. J., Trucks, G. W., Schlegel, H. B., Scuseria, G. E., Robb, M. A., Cheeseman, J. R., Scalmani, G., Barone, V., Mennucci, B., Petersson, G. A., Nakatsuji, H., Caricato, M., Li, X., Hratchian, H. P., Izmaylov, A. F., Bloino, J., Zheng, G., Sonnenberg, J. L., Hada, M., Ehara, M., Toyota, K., Fukuda, R., Hasegawa, J., Ishida, M., Nakajima, T., Honda, Y., Kitao, O., Nakai, H., Vreven, T., Montgomery, J. A., Jr., Peralta, J. E., Ogliaro, F., Bearpark, M., Heyd, J. J., Brothers, E., Kudin, K. N., Staroverov, V. N., Kobayashi, R., Normand, J., Raghavachari, K., Rendell, A., Burant, J. C., Iyengar, S. S., Tomasi, J., Cossi, M., Rega, N.,Millam, J. M., Klene, M., Knox, J. E., Cross, J. B., Bakken, V., Adamo, C., Jaramillo, J., Gomperts, R., Stratmann, R. E., Yazyev, O., Austin, A. J., Cammi, R., Pomelli, C., Ochterski, J. W., Martin, R. L., Morokuma, K., Zakrzewski, V. G., Voth, G. A., Salvador, P., Dannenberg, J. J., Dapprich, S., Daniels, A. D., Farkas, O., Foresman, J. B., Ortiz, J. V., Cioslowski, J., and Fox, D. J.; Gaussian 09, revision D.01; Gaussian Inc.: Wallingford, CT, 2013.
9. Hehre, W. J., Ditchfield, R., and Pople, J. A. (1972). *J. Chem. Phys. 56*, 2257-2261.
10. Zhao, Y., and Truhlar, D. G. (2008). *Theor. Chem. Acc. 120*, 215-241.